

Project Number: DZT-1701

## HUMAN ARTERY PLAQUE PROGRESSION

A Major Qualifying Project Report

Submitted to the Faculty

of the

WORCESTER POLYTECHNIC INSTITUTE

in partial fulfillment of the requirements for the

Degree of Bachelor of Science

in Physics

by

Sayan Mondal

Date: Dec 21, 2007

### Keywords

1. Finite Element Method (FEM)
2. Mechanical Stress/ Strain
3. Atherosclerotic Plaque Progression

Professor Dalin Tang,  
Project Advisor

Professor George Phillies,  
Co-Advisor

## Acknowledgement

I would primarily like to thank my advisor Prof. Dalin Tang, Dept. of Mathematics, WPI for his guidance throughout this project. Thanks to his continued support and with his permission, I have contributed as an undergraduate research assistant to his research project and as a co-author to several peer-reviewed conference papers and a journal paper (*J. Biomechanics*).

I would like to thank Prof. George Phillies, Dept. of Physics, WPI for co-advising this project.

I would like to thank Prof. Tang's research team members Prof. Chun Yuan and Dr. Gador Canton of the University of Washington, Seattle for providing human carotid plaque MRI data. The results obtained in this project owe much of their significance in stroke research to the use of real, *in vivo* data from participating patients.

I would like to thank Prof. Chun Yang of Beijing Normal University, China and Prof. Petruccelli of WPI for helping me on the modeling and the statistical components of the project respectively.

This research was supported in part by the NSF grant DMS-0540684.

## **Abstract**

This project used *in vivo* MRI-based computational models of human carotid atherosclerotic plaques to examine the role of mechanical variables in atherosclerotic plaque progression. It documented quantitative data showing correlation of atherosclerotic plaque progression with structural stress. Further, it developed regression functions for plaque growth in terms of structural stress, arterial wall thickness and plaque history.

# TABLE OF CONTENTS

|   |           |
|---|-----------|
| <b>1. INTRODUCTION.....</b>   | <b>5</b>  |
| 1.1 Problem Statement.....  | 7         |
| 1.2 Data Acquisition.....   | 8         |
| 1.3 The Structure and Fluid Models.....   | 9         |
| <b>2. TWO-DIMENSIONAL MODELING APPROACH.....</b>                                | <b>15</b> |
| 2.1 Finite Element Model of Arterial Cross-section.....                         | 15        |
| 2.2 Shrinking Procedure to Determine Zero-Stress Geometry for 2D Models.....    | 21        |
| 2.3 Determining Arterial Wall Thickness.....                                    | 31        |
| <b>3. RESULTS FROM THE TWO-DIMENSIONAL MODELING APPROACH.....</b>               | <b>36</b> |
| 3.1 Two Time-Point Analysis.....  | 37        |
| 3.2 Three Time-Point Analysis.....  | 42        |
| <b>4. THREE-DIMENSIONAL MODELING APPROACH.....</b>                              | <b>47</b> |
| 4.1 3D Geometry Reconstruction and Meshing.....                                 | 47        |
| 4.2 Solid-Only Model.....   | 55        |
| 4.3 Flow-Only Model.....  | 57        |
| 4.4 Results from the three-dimensional modeling approach.....                   | 58        |
| <b>5. SIGNIFICANCE AND FUTURE DIRECTIONS.....</b>                               | <b>60</b> |
| <b>BIBLIOGRAPHY.....</b>  | <b>63</b> |
| <b>APPENDICES.....</b>  | <b>67</b> |
| A. Matlab Code to Implement the Shrinking Procedure.....                        | 67        |
| B. Determining Area Using Green's Theorem.....                                  | 72        |
| C. Matlab Codes Used to Determine the Arterial Wall Thickness.....              | 73        |
| D. Wall Thickness Increase vs. various components of the structural stress..... | 75        |

# 1. INTRODUCTION

Cardiovascular disease (CVD) is the leading cause of death in the developed world and is expected to become the leading cause of death worldwide by 2020. In the US alone, over 37% of the people (20 years or older) have CVD (AHA statistics, 2007). A major cause of CVD is the build-up and subsequent rupture of atherosclerotic plaque. Lipid, calcium, cellular debris etc. deposit in the arterial walls and accumulate over time to form intra-arterial bodies called plaques. These plaques may grow over time, and may ultimately rupture without warning to cause cardiovascular syndromes such as heart attack and stroke.

The purpose of this MQP was to study human carotid atherosclerotic plaque progression by using computational models based on multi-year patient-specific magnetic resonance imaging (MRI) data. Atherosclerotic plaque progression is a multi-faceted process involving mechanical forces, plaque morphology and inflammation, vessel remodeling, blood conditions, chemical environment, lumen surface condition, and genetic factors (Berlinger, et al., 1995; Friedman, 1987, 1993; Giddens et al., 1993; Indolfi, 2002; Ku, 1997; Ku et al., 1985; Naghavi et al., 2003a, 2003b; Ravn and Falk, 1999). This project concerned itself with the mechanical factors involved in atherosclerotic plaque growth.

In this project, 2D and 3D patient-specific Finite Element models based on multi-year *in vivo* MR images of the carotid artery of 11 human patients were used to obtain flow shear stress and structural stress/strain distributions in the plaque and quantify possible correlations between atherosclerotic plaque progression and mechanical variables. Patient-specific plaque growth functions were determined based on the correlations found.

Several groups have previously attempted to simulate mechanical stress-induced plaque growth (for example, Humphrey and Rajagopal, 2002a; Kuhl et al., 2006). Their models attempted to computationally simulate the continuous growth process. However, arteries are living organs that can adapt to and change with varying conditions (Ku, 1997). It is difficult to use such growth simulation models to capture the vitality of the biological response to changing mechanical conditions. Unlike these papers, this project used real plaque growth data obtained from snapshots of the artery at discrete time points (about 1 to 1.5 years apart). FEM models provided snapshots of the distribution of the mechanical factors in the artery at these discrete time points. This information was used to statistically quantify human plaque growth functions. Fig. 1.1 shows the geometry of a human carotid artery at two discrete time points for illustration.

This is the first time that quantitative human plaque growth functions have been quantified. These growth functions can be used to simulate plaque progression and make patient-specific predictions.

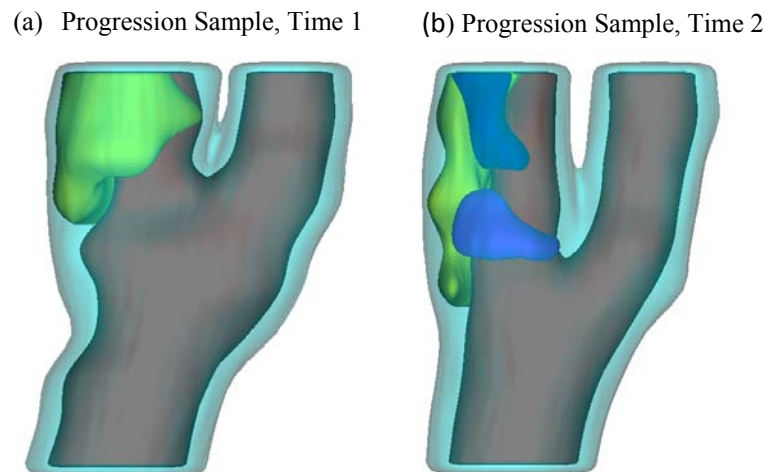


*Fig. 1.1 A diseased carotid artery, reconstructed from MRI images, at time 1 and time 2 (about 18 months apart).  
Transparent Blue: Outer Wall, Green: Lipid, Blue: Calcification, Brown: Inner wall.*

## 1.1 Problem Statement

According to a widely accepted hypothesis, low and oscillating flow wall shear stress creates conditions favorable to atherosclerotic plaque initiation and progression (Ku, 1997). However, as the plaque grows, the lumen narrows leading to increase in blood shear stress conditions. Yet, the plaque continues to grow under this elevated condition of flow wall shear stress. Therefore, this hypothesis cannot fully explain plaque progression.

We may look beyond the flow mechanical variables, and investigate if the structural mechanical variables play any role. Prof. Tang's research group came up with a new hypothesis that low structural stress may be associated with plaque progression, and may create favorable mechanical conditions in the artery for intermediate and advanced plaque progression. This project sought to test this new hypothesis.

This project investigated possible correlations between plaque maximum principal stress and plaque progression. In order to test this hypothesis, this project quantified the correlations between local plaque progression, as estimated by the local Wall Thickness Increase (WTI), and the local  $\sigma_{P1}$ . Several past research papers have used WTI to approximate plaque growth (for example, Kuhl et al., 2006).

Furthermore, this project developed plaque growth functions in terms of  $\sigma_{P1}$ . This is the first time that human atherosclerotic plaque growth has been quantified. The correlations of WTI with certain other mechanical variables are also reported.

This document also reports a form of dependence of plaque growth on mechanical stress, arterial wall thickness and plaque history that consistently explained a high percentage of the

variability in plaque progression in all arterial cross- sections for which MRI data was available. This may be an important discovery, and may ultimately help to simulate plaque progression.

## 1.2 Data Acquisition

This project utilized *in vivo* MRI images of carotid artery from human patients. The results reported here are particularly relevant in stroke research because of this use of *in vivo* human data; this made it possible to estimate the actual plaque growth in the living body of the patient under consideration, and to make patient-specific finite element models.

The *in vivo* MRI images of human carotid atherosclerotic plaques were provided by Dr. Yuan and his group at the University of Washington, Seattle using a protocol approved by the University of Washington Institutional Review Board with informed consent obtained. MRI scans were conducted on a GE SIGNA 1.5T whole body scanner using the protocol outlined in Yuan and Kerwin (2004). A carotid phased array coil was used for all scans. Multi-contrast images in T1, T2, proton density (PD), time-of-flight (TOF), and contrast-enhanced (CE) T1 weightings of carotid atherosclerosis were generated to characterize plaque tissue composition, luminal and vessel wall morphology. The MRI scans of the artery were taken at intervals of 2mm. The scan parameters used were: Matrix Size= 512\*512, and Field of Vision= 160mm\*160mm. A computer package CASCADE (Computer-Aided System for Cardiovascular Disease Evaluation) developed by the Vascular Imaging Laboratory (VIL) at the University of Washington (UW) was used to perform image analysis and segmentation. CASCADE allows for all contrast weightings to be simultaneously displayed, indexed relative to the carotid bifurcation, and analyzed serially along the length of the carotid artery. Fig. 1.2 gives a screen shot of a CASCADE display showing multiple contrast weighting MR images with contours generated by CASCADE.

CASCADE provides manual and automatic analysis tools for accurate lumen and wall boundary detection, and image registration. A histologically validated automated *in vivo* plaque composition algorithm – MEPPS (Morphology-Enhanced Probabilistic Plaque Segmentation) facilitated the analysis of plaque components which include lipid-rich necrotic core (including intraplaque hemorrhage), calcifications, loose matrix (including all tissues that were loosely woven, such as proteoglycan rich fibrous matrix, organizing thrombus, and granulomas), and others. Upon completion of a review, an extensive report was generated and segmented contour lines for different plaque components for each slice were stored as digital files for 2D and 3D geometry reconstruction.

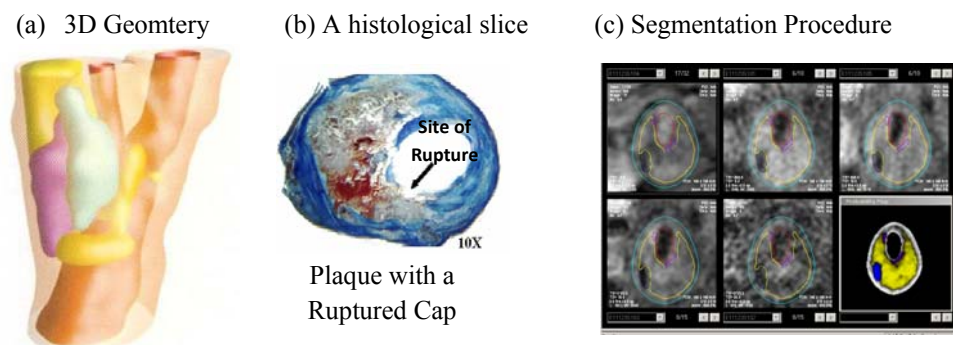


*Fig. 1.2 (a) A typical 3D human carotid artery plaque re-constructed from MR images exhibiting calcification (light blue) and intraplaque hemorrhage (purple) in addition to a lipid core (yellow); (b) a histological slice showing site of rupture; (c) CASCADE multi-weighting segmentation procedure.*

### 1.3 The Structure and Fluid Models

This section presents the generic mathematical formulation of the solid model for the arterial material and the plaque components, and the fluid model for the blood flow through the artery. This formulation would be next used to construct patient-specific Finite Element models.

### 1.3.1 Solid Model

The solid model was formulated using the theory of non-linear elasticity for large deformations.

The artery and the plaque components were assumed to be:

- Hyperelastic- The material does not have significant memory
- Isotropic- The stiffness at every point is the same in all directions
- Incompressible- The total volume of the material is conserved when the body is stretched or compressed

In particular, the material was modeled by the non-linear Mooney-Rivlin hyperelastic model (Huang et al., 2001; Tang et al., 2004). The non-linear Mooney-Rivlin model successfully captures the stiffening behavior of the arterial material with increasing strain (fig. 1.3), and matches well with experimental results (Huang et al., 2001).

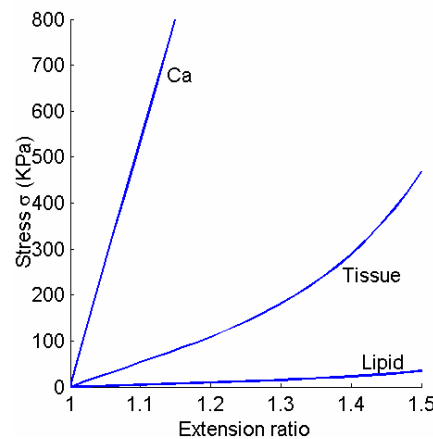


*Fig. 1.3 Typical material curves for Arterial Tissue, Lipid and Calcium. The material is modeled by the Mooney-Rivlin model. The model captures the stiffening behavior of the artery with increasing strain.*

The hyperelastic, isotropic effects are mathematically described by the relation between the strain energy density  $W$  and the deformation tensor  $C$ . This relation mathematically defines the nature of the material.

The strain energy function that defines the Mooney-Rivlin model is given by:

$$W = c_1(I_1 - 3) + c_2(I_2 - 3) + D_1[\exp(D_2(I_1 - 3)) - 1], \quad (1.1)$$

where the Strain Invariants  $I_1 = C_{ii}$ ,  $I_2 = \frac{1}{2}[I_1^2 - C_{ij}C_{ij}]$ . (For an incompressible material,  $I_3 = 1$ )

$C = \mathbf{X}^T \mathbf{X}$  is the right Cauchy-Green deformation tensor,  $\mathbf{X} = [X_{ij}] = \left[ \frac{\partial x_i}{\partial a_j} \right]$ , ( $x_i$ ) being the current position, ( $a_j$ ) being the original position of the deformation tensor.

The choice of values for the parameters  $c_1$ ,  $c_2$ ,  $D_1$ ,  $D_2$  define the material for the artery. Stiffer materials would have larger values for these parameters. The stiffness of the lipid pool is about 1/100 times that of the normal arterial tissue. The calcification is treated to be about 10 times stiffer than the normal arterial tissue. Tang et al. (2004) found that variations of lipid and calcification stiffness (reduction by 50% or increase by 100%, preserving the ratios) had less than 2% impact on the simulation results for the samples considered in that paper (one 3D and eleven 2D samples). The parameter values used in this project were:

$$\text{Normal Arterial Tissue: } C_1 = 368000.0, C_2 = 0, D_1 = 144000.0, D_2 = 2.0$$

$$\text{Lipid: } C_1 = 20000.0, C_2 = 0, D_1 = 20000.0, D_2 = 1.5$$

$$\text{Calcification: } C_1 = 3680000, C_2 = 0, D_1 = 1440000.0, D_2 = 2.0$$

The units for  $C_1$  and  $D_1$  are dyne/sq.cm.  $D_2$  is dimensionless.

The Cauchy-Green Deformation tensor  $C$  is related to the Green-Lagrange strain tensor  $\epsilon$  as:

$$C_{ij} = 2\epsilon_{ij} + \delta_{ij}, \quad (1.2)$$

where  $\delta$  is the Kronecker delta.

The complete solid model using the Einstein summation convention is the following  
(Tang et al., 2004):

**Equation of motion for solids:**

$$\rho v_{i,tt} = \sigma_{ij,j}, \quad (1.3)$$

where  $i,j=1,2,3$ ;  $t$  is the time,  $i$  and  $j$  label spatial coordinates,  $\mathbf{v}$  is the solid deformation vector,  $\boldsymbol{\sigma}$  is the 2<sup>nd</sup> Piola-Kirchoff stress tensor;  $f_{,j}$  is the derivative of  $f$  with respect to the  $j$ th variable.

**Strain-Displacement Relation:**

$$\varepsilon_{ij} = \frac{1}{2} (v_{i,j} + v_{j,i}), \quad (1.4)$$

where  $i,j=1,2,3$  and  $\boldsymbol{\varepsilon}$  is the strain tensor

**Boundary Conditions (balance of stresses and continuity of displacement):**

$$\sigma_{ij} \cdot n_{j|out\_wall} = 0, \quad (1.5)$$

$$\sigma^{(r)}_{ij} \cdot n_{j|interface} = \sigma^{(s)}_{ij} \cdot n_{j|interface}, \quad (1.6)$$

$$\mathbf{u}^{(r)}|_{interface} = \mathbf{u}^{(s)}|_{interface}, \quad (1.7)$$

where the superscripts  $r, s$  indicate different materials.

**Strain Energy Density:**

$$W = c_1(I_1 - 3) + c_2(I_2 - 3) + D_1[\exp(D_2(I_1 - 3)) - 1] \quad (1.8)$$

**Stress-Strain Relationship:**

$$\sigma_{ij} = \frac{1}{2} (\partial W / \partial \varepsilon_{ij} + \partial W / \partial \varepsilon_{ji}) \quad (1.9)$$

### 1.3.2 Flow Model

The blood flow was assumed to be laminar, viscous, incompressible and Newtonian. A no-slip boundary condition is assumed at the fluid-solid interfaces.

Note that blood flow is in general non-Newtonian. However, the non-Newtonian nature of blood flow is important mainly in microcirculatory systems or if the flow shear stress is very low (leading to clumping of the red blood cells). In most arteries, blood behaves in a Newtonian fashion with a constant viscosity of 4 centipoise (Ku, 1997).

The Navier-Stokes equations were used as the governing equations for blood flow. More precisely, Navier-Stokes equations with the arbitrary Lagrange-Eulerian formulation (ALE) were used.

For flow through a rigid pipe, we may use the Eulerian approach to formulate the problem whereby we would focus on the flow through a fixed volume of the vessel. However, in our case, the arterial vessel deforms leading to deforming boundary of the flow. Therefore, there is no fixed volume of the flow to focus on, and the Eulerian approach would fail.

The opposite of the Eulerian approach is the Lagrangian approach whereby the reference frame would move at the velocity of the flow at each point. However, we would use finite element methods (FEM) to solve the model and if the finite elements mesh were to move at the same velocity as the fluid at each node, then this would lead to undesirably large mesh deformations.

Therefore, we use the Arbitrary Eulerian-Lagrangian (ALE) formulation. In the ALE formulation, the reference frame moves at a velocity less than that of the fluid at that point.

As the finite element mesh moves, the volume of each cell in the grid changes and the fluid mass is not conserved for each individual cell. This is accounted for by using the Geometry Conservation Law that leads to

$$\text{Cell Volume}_{|\text{new}} - \text{Cell Volume}_{|\text{old}} = \int_V \nabla \cdot \mathbf{u} \, dV \quad (1.10)$$

Eq. 1.10 accordingly modifies the equation of continuity for individual cells in the finite element model.

The complete flow model is given by:

**Navier-Stokes Equations with ALE formulation:**

$$\rho(\partial \mathbf{u} / \partial t + ((\mathbf{u} - \mathbf{u}_g) \cdot \nabla) \mathbf{u}) = -\nabla p + \mu \nabla^2 \mathbf{u}, \quad (1.11)$$

where  $\mathbf{u}$  is the flow velocity,  $\mathbf{u}_g$  is the mesh velocity,  $\mu$  the coefficient of viscosity,  $p$  the pressure and  $\rho$  the density.

**Equation of Continuity:**

$$\nabla \cdot \mathbf{v} = 0 \quad (1.12)$$

**Boundary Conditions:**

$$\mathbf{v}|_{\Gamma} = \partial \mathbf{x} / \partial t, \quad \partial \mathbf{v} / \partial \mathbf{n}|_{\text{inlet, outlet}} = 0, \quad (1.13)$$

$$p|_{\text{inlet}} = p_{\text{in}}(t), \quad p|_{\text{outlet}} = p_{\text{out}}(t), \quad (1.14)$$

where  $\Gamma$  represents the inner wall of the vessel.

## **2. TWO-DIMENSIONAL MODELING APPROACH**

The problem was investigated at the two-dimensional level, i.e., each carotid artery was modeled at equi-spaced cross-sections 2mm apart. This chapter describes the construction of patient-specific two-dimensional Finite Element models.

The two-dimensional modeling approach is simpler than the full-blown three-dimensional modeling approach, consumes less computational runtime, and provides preliminary results.

It is also to be noted that a two-dimensional model of the artery does not include the shear effect of blood flow through the artery. So, a two-dimensional model is a theoretical simplification that ignores Fluid Structure Interaction (FSI) between the flowing blood and the artery. Therefore, this analysis will, in some sense, help to isolate the effect of structural stress on plaque thickness increase, which is the objective of this project.

### **2.1 Finite Element Model of Arterial Cross-section**

For each cross-section, a 2D FEM model was constructed using the structural modeling component of the finite element package Adina. This section describes the procedure for doing so.

### 2.1.1 Pre-processing Stage

The first step was to construct the model geometry. We begin with a segmented MR image of each arterial cross-section. Therefore, we have the coordinates of the arterial data points, and know which points belong to the arterial walls, which points belong to the calcification, and so on.

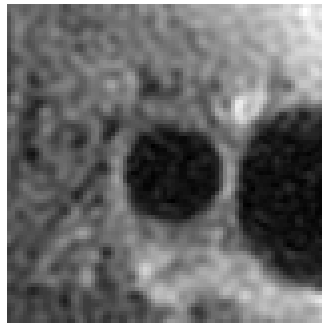


*Fig. 2.1 MR Image of a cross-section of an artery*

These geometry key points were imported into Adina, and entered on the Y-Z plane. The contour of the outer wall was constructed by joining its key points into a smooth, closed line. A cubic spline interpolation was used to do this. The contours for the inner wall, calcification, lipid, and other arterial components were similarly constructed.

The contours were next used to define corresponding 2D sheet-type bodies for each component (Ca, lipid, main arterial body, etc.) of the arterial cross- section.

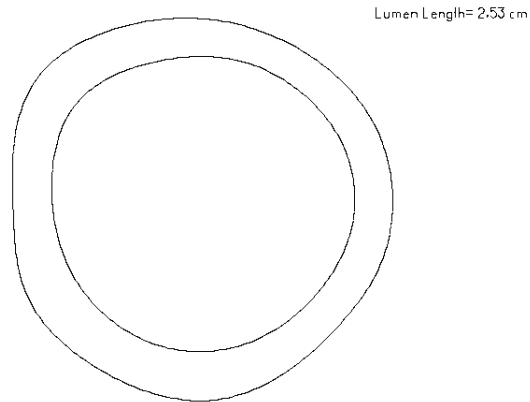


*Fig. 2.2 Geometry for a 2D model of an arterial cross-section.*

The second step was to define the material properties. As mentioned in Ch. 1, the non-linear Mooney-Rivlin model was used to model the material of the artery and its components. The choice of the parameters  $c_1$ ,  $c_2$ ,  $D_1$ ,  $D_2$  define the material were selected to match experimental results and current literature (Humphrey, 2002; Kobayashi et al., 2003).

Note that calcification is stiffer than arterial material, while arterial material is stiffer than lipid. As a modeling simplification, the other components such as hemorrhage were ignored, i.e., their material was modeled with the parameter values of the normal arterial material.

The boundary condition and the loading were next specified. The 2D solid is in the Y-Z plane. The X, Y and Z degrees of rotation as well as the X- degree of translation were constrained. No boundary condition was otherwise imposed on the model boundary. The loading was specified as a uniformly distributed normal pressure on the lumen boundary. The magnitude of the pressure was chosen to be the systolic blood pressure of the specific patient. The pressure was applied in 20 incremental time steps. The numerical model converges stepwise if the pressure is incrementally applied in steps, but will not converge if the entire pressure is applied in one single step.

The next step is to set up the mesh for plane stress analysis. Corresponding to each of the three types of material, an element group was defined. 2D plane stress type of element was chosen for each group. This choice has two implications: first,  $\sigma_{xx}=\sigma_{yy}=\sigma_{zz}=0$ ; second, the material is treated as incompressible. Large displacements were assumed for the kinematic formulation for each element group. Each edge was subdivided into 100 equal subdivisions. To the face of each body, the element group of the appropriate material type was associated, and the face was meshed with 9-node quadrilateral elements.

### 2.1.2 Processing Stage

The model was processed with the following controls:

Large strain/large displacements were assumed.

A non- linear static analysis was performed. The equilibrium equations to be solved are

$$\mathbf{R}_{t+\Delta t}-\mathbf{F}_{t+\Delta t}=\mathbf{0} \quad (2.1)$$

where  $\mathbf{R}_{t+\Delta t}$  is the vector of externally applied nodal loads at time  $t+\Delta t$ , and  $\mathbf{F}_{t+\Delta t}$  is the vector of force vector equivalent to the element stresses at time  $t+\Delta t$ .

The full Newton iteration scheme was used. The iteration equations are

$$\mathbf{K}^{(i-1)}_{t+\Delta t} \Delta \mathbf{U}^{(i)} = \mathbf{R}_{t+\Delta t} - \mathbf{F}^{(i-1)}_{t+\Delta t} \quad (2.2)$$

$$\mathbf{U}^{(i)}_{(t+\Delta t)} = \mathbf{U}^{(i-1)}_{t+\Delta t} + \Delta \mathbf{U}^{(i)} \quad (2.3)$$

where  $K_{t+\Delta t}^{(i-1)}$  is the stiffness matrix at the end of the (i-1) th iteration at time  $t+\Delta t$ , and  $U$  is the incremental displacement vector.

Automatic Time Stepping (ATS) was used, with maximum number of iterations = 50. Energy is used as the convergence criteria, with a tolerance level of 0.005, i.e, convergence criteria is satisfied for

$$\frac{\Delta U^{(i)}[R_{t+\Delta t} - F_{t+\Delta t}^{(i-1)}]}{\Delta U^{(1)}[R_{t+\Delta t} - F_t]} < 0.005 \quad (2.4)$$

### 2.1.3 Post-processing Stage

The processed model approximates the arterial distributions of specific mechanical variables, such as the maximum principal value  $\sigma_{p1}$  of the stress tensor.

The numerical model was first tested for mesh invariance with respect to  $\sigma_{p1}$  in order to test for convergence. The model was reprocessed with a finer mesh, and the distributions of  $\sigma_{p1}$  and the maximum value of  $\sigma_{p1}$  compared between the models with different meshes.

If the numerical model is found to be mesh invariant with respect to  $\sigma_{p1}$ , we can then obtain the values of the selected mechanical variables at the nodes on the lumen boundary (and at other nodes, if we want those values.)

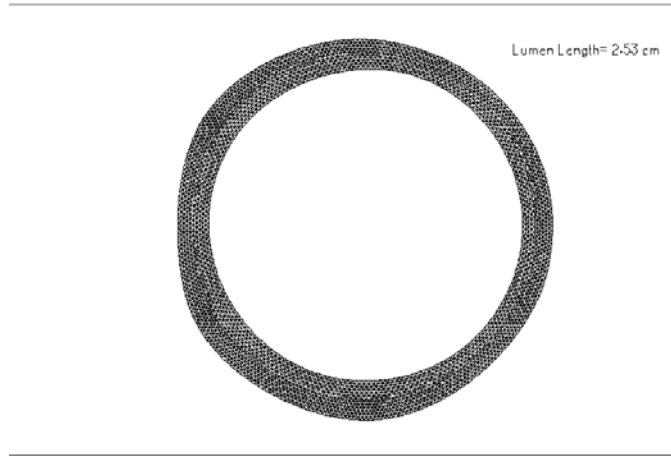


Fig. 2.3 A Deformed Mesh

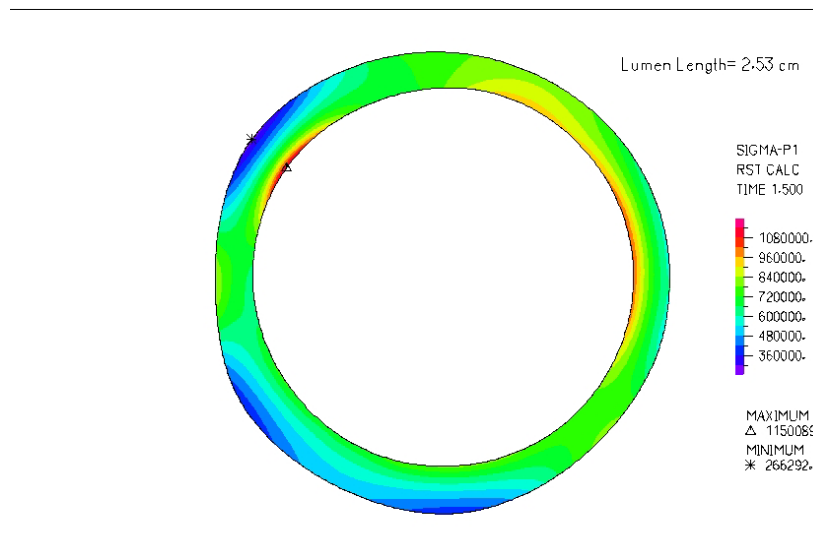


Fig. 2.4 Band plot for the maximum principal value of the Stress tensor  $\sigma_{P1}$

Now, the applied normal pressure deforms the original mesh. However, we are here trying to simulate the *in vivo* arterial cross-section; as such, we want the *deformed* mesh to resemble the actual *in vivo* arterial cross-section. Therefore, we need to start out with an arterial contour that would deform to the *in vivo* geometry observed in the MRI.

Therefore, the geometry key points that we need to start out with for the model are actually not exactly the same as that of the corresponding MR image of the *in vivo* artery. To obtain the starting model geometry from the *in vivo* MR image, the MR image is shrunk by a patient-specific percentage such that when the patient-specific blood pressure is applied to this geometry, it expands to the *in vivo* geometry.

## **2.2 Shrinking Procedure to Determine Zero-Stress Geometry for 2D Models**

As explained in the previous section, each 2-D slice was shrunk in order to generate an approximation to its zero-stress geometry. This section explains the shrinking procedure, which was implemented using the Matlab code presented in Appendix A.

A key feature of the shrinking procedure is that it ensures mass conservation in generating the zero-stress geometry. The 2-D slices are assumed to have homogenous arterial material and components. Therefore, conservation of mass is manifested as conservation of area for the 2D vessel and each component.

The Matlab code first converts the MRI data points from units of pixel to units of cm and store them in appropriate matrices. The 2D slice is then shrunk using the following four-part procedure:

A. Determining the percentage by which the lumen needs to be shrunk by performing a numerical experiment using Adina.

B. Determining the percentage by which the outer wall needs to be shrunk in order to conserve the cross-section area of the artery.

C. Calculating the final coordinates of the nodal points of inner and outer boundaries of the artery cross section.

D. Determining the location of each component (lipid, calcification etc.) in the zero-stress geometry, without changing the component area.

### **2.2.1 Determining the shrinkage percentage for the Inner Wall**

The following criterion is used in determining the shrinkage percentage for the lumen:

- When the appropriate patient-specific pressure is applied at the lumen of the zero-state geometry, the lumen circumference must increase to within 1% of the lumen circumference observed in the MRI.

This part of the procedure is performed via the following steps:

1. The 2D FEM model is run in Adina using the original geometry points and the patient-specific pressure.
2. The percentage by which the lumen expands in step 1 is noted. This is used to obtain a starting shrinkage percentage for the lumen. For example, if the lumen circumference is found to expand by 20%, then the starting shrinkage percentage for the lumen is  $(100/120)*100\%$  which is about 83%.
3. For the given shrinkage of the lumen, the shrunk geometry is determined using steps B, C and D (described below). The model is then run in Adina using the shrunk geometry as the starting unstressed configuration and the same pressure loading.

4. On applying the pressure, the lumen expands. The length of the expanded lumen is obtained and compared to the original lumen length, and the shrinkage for the lumen is adjusted accordingly. For example, if the expanded lumen length is greater than the original lumen length, then we need to shrink the lumen a little more.

5. Steps 3 and 4 are repeated for the new shrinkage. The iterations are continued till the criterion is satisfied.

This process usually converges within 3-4 iterations. The determination of the shrinkage percentage is performed for only one slice per artery. The shrinkage percentage obtained from the numerical experiment with that slice is used for all the slices in that particular artery.

### **2.2.2 Determining the shrinkage percentage for the outer wall**

This part of the procedure accepts as input the shrinkage percentage for the lumen, and determines the percentage by which the wall needs to be shrunk in order to conserve the area of the slice. It does so via the following steps:

1. The lumen is shrunk by multiplying its coordinates by a factor  $f$  ( $f < 1$ ).

$$\begin{aligned}x\_shrunk &= f * x \\y\_shrunk &= f * y\end{aligned}\tag{2.5}$$

The value of  $f$  is defined by the shrinkage percentage of the lumen (Part A). For example, if it needs to be shrunk by 20%, then  $f=0.8$

2. This step determines the area enclosed by the contours of the original lumen ( $A_{Lumen}$ ), the shrunk lumen ( $A_{Shrunk\_Lumen}$ ), and the original wall ( $A_{Wall}$ ) respectively. Using Green's theorem, the signed area enclosed by a simple, closed curve  $C:y=f(x)$  is expressed as

$$Area = \frac{1}{2} \left( \int_C x dy - \int_C y dx \right) \quad (2.6)$$

The line integrals in Eq. 2.6 are computed using Matlab's inbuilt trapezoidal integration routine.

The area of the artery at the cross-section is then given by

$$A = A_{Wall} - A_{Lumen} \quad (2.7)$$

We need to conserve this area  $A$  in the shrinking process.

The area of the vessel at the cross-section with the lumen shrunk is given by

$$A_{Shrunk} = A_{Wall} - A_{Shrunk\_Lumen} \quad (2.8)$$

Now,  $A_{Shrunk\_Lumen} < A_{Lumen}$ , and so,  $A_{Shrunk} > A$ . Therefore,  $A_{Wall}$  needs to be decreased by shrinking the wall by such a percentage that  $A_{Shrunk} \approx A$ . This is done in the next step.

3. The original coordinates of the wall are multiplied by a factor  $b$ .

$$\begin{aligned} x_{wall\_new} &= b * x \\ y_{wall\_new} &= b * y \end{aligned} \quad (2.9)$$

This step will determine an appropriate value of  $b$ . The value of  $b$  is initialized with  $b=1$ . For a given value of  $b$ ,  $A_{Shrunk}$  is determined and compared to the original area  $A$ . If the difference exceeds a tolerance level (set to 1% of the original area),  $b$  is slightly decreased (by

0.005) and this step is repeated. The iterations continue till the discrepancy between  $A$  and  $A_{\text{Shrunk}}$  is within the tolerance level. The value of  $b$  is thus determined.

### C. Determining the final coordinates of the wall and the lumen

The process of shrinking the outer wall and the lumen by different percentages causes the lumen to be dislocated relative to the wall (fig. 2.5).

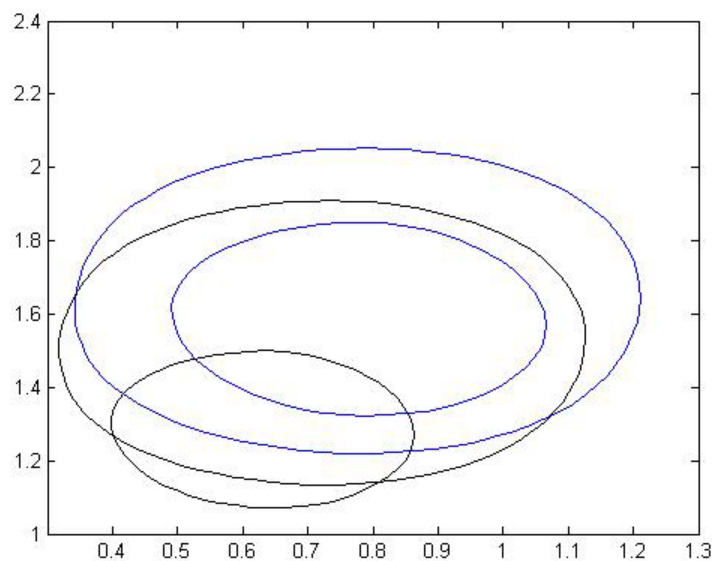


*Fig. 2.5 Shrinking the outer wall and the lumen contours by different percentages dislocates the lumen w.r.t. the wall. Blue: original contours. Black: shrunk contours. The component is not shown in this figure.*

This part of the code restores the relative position of the lumen and the wall. It does so by translating the shrunk lumen such that the centroid of the translated lumen coincides with that of the original lumen, and translating the shrunk wall such that the centroid of the shrunk wall coincides with that of the original wall.

The coordinates  $(X,Y)$  of the centroid of an area  $A$  is defined by

$$X = \frac{\iint_A x dA}{A} \quad (2.10a)$$

$$Y = \frac{\iint_A y dA}{A} \quad (2.10b)$$

Green's theorem is used to reduce the double integrals in Eq. 2.10 to line integrals around the contour enclosing the area A. This leads to the following expressions for X and Y:

$$X = \frac{\int_C x^2 dy}{2A} \quad (2.11a)$$

$$Y = -\frac{\int_C y^2 dx}{2A} \quad (2.11b)$$

In determining X and Y using Eq. 2.11, the area A is obtained from Step 2 while the line integrals are once again computed using Matlab's inbuilt trapezoidal numerical integration routine.

The centroids of the original wall, shrunk wall, original lumen and the shrunk lumen are first determined using Eq. 2.11. This information is then used to generate the final coordinates of the shrunk wall and the lumen. Eq. 2.12 presents how the final coordinates of the outer wall contour are determined.

$$dx\_wall = X\_wall\_original - X\_wall\_new$$

$$x\_wall\_final = x\_wall\_new + dx\_wall$$

(2.12)

$$dy\_wall = Y\_wall\_original - Y\_wall\_new$$

$$y\_wall\_final = y\_wall\_new + dy\_wall$$

Here, X and Y refer to the centroid coordinates whereas x and y refer to the contour coordinates. The final coordinates of the lumen are similarly determined using the centroids of the shrunk and the original lumen.

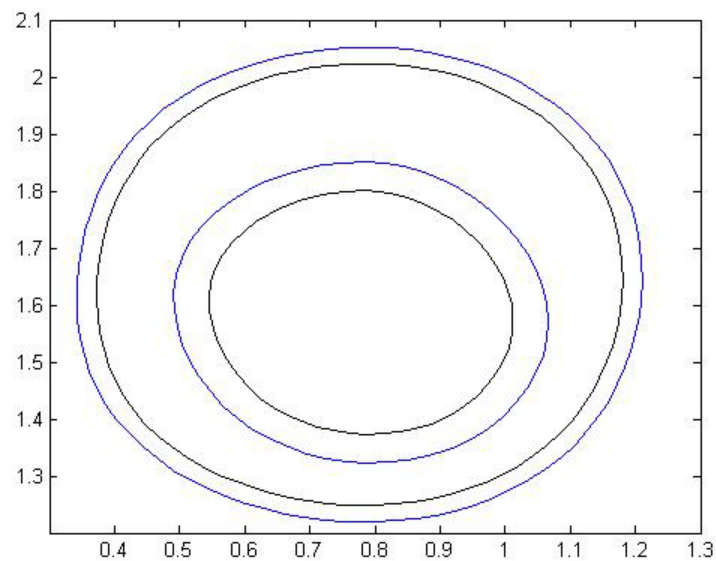


*Fig. 2.6 The relative positions of the lumen and the wall contours are restored. Blue: original contour. Black: Shrunk contour. The component is not shown in this figure.*

### **2.2.3 Determining the location of each inclusion in the shrunk vessel**

This part of the code adjusts the position of the each inclusion such that its “relative” location inside the vessel remains “unchanged”.

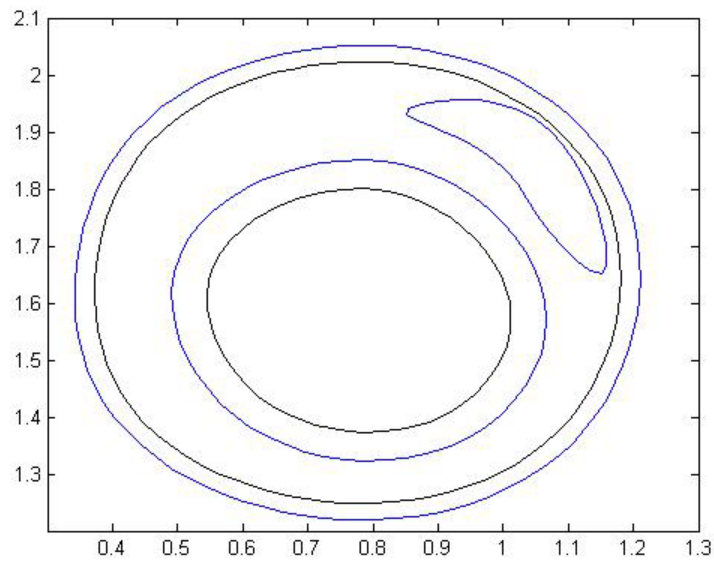


*Fig. 2.7 The position of the lipid component next needs to be adjusted. Blue: original contours. Black: shrunk contours*

This part of the procedure has the following key features:

- The area of each component is conserved.
- Each component occupies the same angular region that it originally occupied.
- The new location of each component is determined as per some objective criteria.

This part of the code adjusts the inclusion position via following steps:

1. The coordinates of the inclusion are first converted from Cartesian to polar with respect to the **centroid of the lumen area**.
2. The two “extreme” points of the component are determined (fig. 2.8). This splits the component contour into two parts: Part 1 near the lumen and Part 2 away from the

lumen.

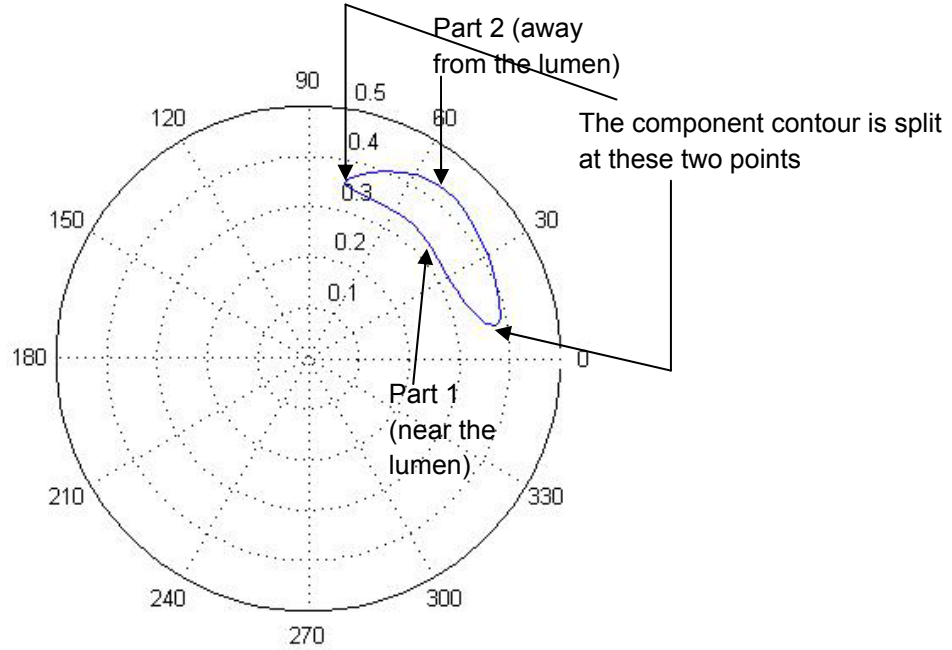


Fig. 2.8 Showing the lipid component in the polar grid. The center of the polar grid is at the centroid of the lumen.

3. The polar radii of the points on part 1 of the contour are to be shrunk by multiplying by a factor  $d_1$ . The polar radii of the points on part 2 of the contour are to be shrunk by multiplying by a factor  $d_2$ .
4. Now, based on the criteria used to move the inclusion (to be discussed next), **either**  $d_1$  **or**  $d_2$  is fixed.
5. The code determines a value for the other factor (of  $d_1$  and  $d_2$ ) that conserves the area of the component.
6. The shrunk polar coordinates are then converted back to Cartesian. The final coordinates of the component are thus obtained.

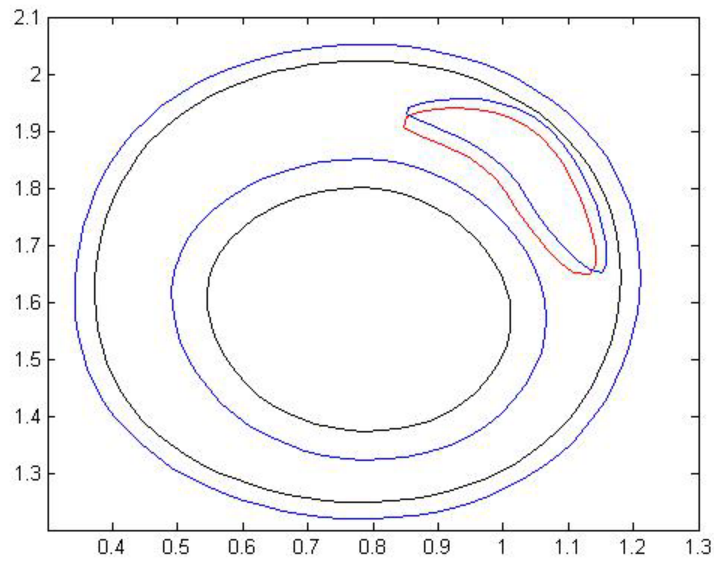


Fig. 2.9 The original and the final shrunk contours. Blue: original contours. Black/ red: final contours.

**Criteria for fixing  $d_1$  or  $d_2$ :**

There appear to be three alternative criteria to fix one of the two factors ( $d_1$  or  $d_2$ ):

1. Preserve (approximately) the gap between Part 2 of the component and the outer wall. This is implemented by fixing  $d_2=b$ , where  $b$  was the factor by which the original coordinates of the wall was multiplied in order to shrink it.
2. Preserve the gap between Part 1 of the component and the lumen. This is implemented by fixing  $d_1=f$ , where  $f$  was the factor by which the original coordinates of the lumen was multiplied in order to shrink it.
3. Preserve the gap between Part 2 of the component and the lumen. This is implemented by fixing  $d_2=f$ .

## 2.3 Determining Arterial Wall Thickness

It may be recalled from Chapter 1 that the local plaque growth from time 1 to time 2 was estimated as the increase in the local arterial wall thickness. This section presents and compares possible definitions for the arterial wall thickness at a given point on the inner wall of the artery.

For each cross-section of the artery, the vessel thickness is determined at 100 equi-spaced points on the lumen boundary. These points correspond to the nodes at which the values of the various mechanical variables were determined using the corresponding finite element model.

For a given arterial slice, we start with the coordinates of the nodes on the outer wall and the lumen. In order to determine the wall thickness at a given node  $N_L$  on the lumen, we need to pair it up with a corresponding node  $N_W$  on the wall such that distance  $(N_L, N_W)$  represents the arterial thickness at  $N_L$ .

There are conceivably three ways of doing this, each of which corresponds to a somewhat different definition of wall thickness.

### 1. Thickness Normal to the Lumen:

Let  $N_{L,1}$  be the node immediately next to  $N_L$ . Then,  $N_W$  is selected such that the line segment  $N_W N_L$  is approximately normal to the line segment  $N_L N_{L,1}$ .

My code implements this definition as follows: It first determines the scalar product  $\mathbf{N}_{W,i} \cdot \mathbf{N}_L - \mathbf{N}_L \mathbf{N}_{L,1}$  for a number of consecutive outer wall nodes  $N_{W,i}$ . Then, it selects the  $N_{W,i}$  for which  $|\mathbf{N}_{W,i} \cdot \mathbf{N}_L - \mathbf{N}_L \mathbf{N}_{L,1}|$  is minimum. Appropriate bounds are placed to prevent the diametrically opposite node from being selected.

Steinman et al. (2002), for example, has used the concept of thickness normal to the lumen to determine arterial thickness.

Drawback: For parts of the lumen that are concave (with respect to its centroid), this method does not seem to yield a reasonable thickness. Fig. 2.10 illustrates this problem.

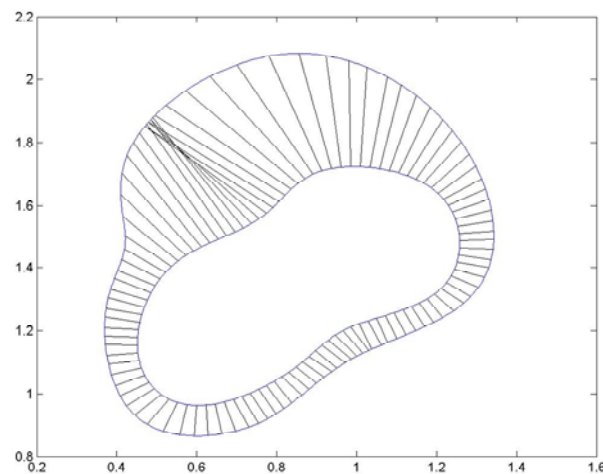


*Fig. 2.10 Determining Local Arterial Wall Thickness Normal to the Lumen. Each black line segment pairs a node on the lumen with an appropriate node on the outer wall. Note: For the two parts of the lumen that are concave with respect to the lumen centroid, the thickness obtained may not be the best possible option.*

## **2. Shortest Distance to the Outer Wall:**

In this method, the distances between  $N_L$  and the outer wall nodes  $N_{W,i}$  (within a certain angular region containing  $N_L$ ) are determined, and the shortest distance is selected as the wall thickness at  $N_L$ .

My code implements this method as follows:

- i) The centroid of the lumen is determined using Eq. 25 from chapter 2, and a polar coordinate system is defined with its center at the centroid of the lumen.

- ii) Let the polar angle of  $N_L$  be  $\alpha$ . Then, all the  $N_{W,i}$  with polar angles between  $\alpha \pm d\alpha$  are selected. The parameter  $d\alpha$  can be chosen as desired; fig. 2.11 illustrates the effect of choice of  $d\alpha$ .

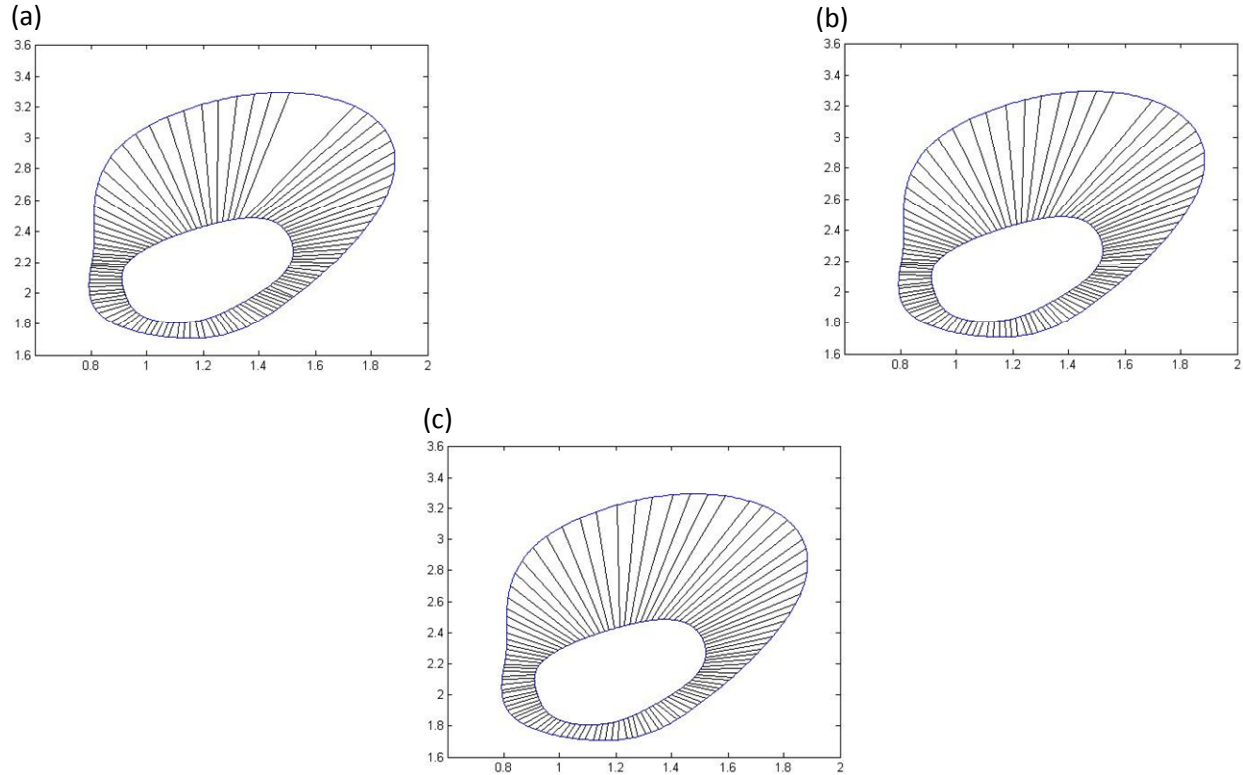
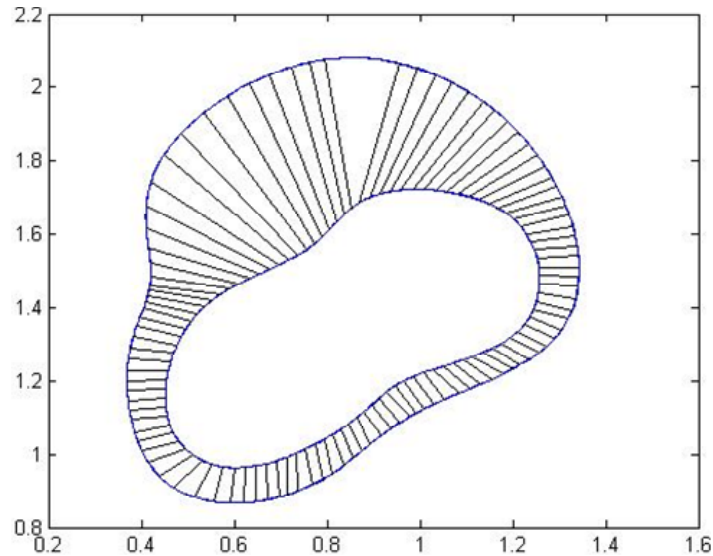


Fig. 2.11 Determining arterial wall thickness as the shortest distance to the outer wall: the effect of the choice of  $d\alpha$ . (a)  $d\alpha=5$  degree, Max thickness= 0.832, (b)  $d\alpha=2.5$  degree, Max thickness= 0.840, (c)  $d\alpha=1.0$  degree, Max Thickness=0.8445 cm. Reducing the value specified for  $d\alpha$  appears to make the process more reactive to the shape, and less sensitive to the idea of "shortest distance".

- iii) Finally, for each  $N_{W,i}$ , the distance  $(N_L, N_{W,i})$  is determined. Then, the  $N_W$  corresponds to the  $N_{W,i}$  for which this distance is shortest.

Underhill et al. (2006), for example, has used the concept of shortest distance to the outer wall to determine the arterial thickness.

Drawback- In the regions where the curvatures of the lumen and the outer wall differ a lot, this method does not seem to yield reasonable thicknesses. Fig. 2.12 illustrates this problem. However, this problem can be somewhat reduced by decreasing the magnitude of  $d\alpha$ .



*Fig. 2.12 Drawback in determining arterial wall thickness as the shortest distance to the outer wall.*

Therefore, while both these methods do work up to a certain extent, there are drawbacks associated with these methods arising from their inability to handle some aspect or the other of the irregularity of the arterial geometry. We here propose a novel third method that is a modification of the second method, and that better handles the irregularity of the arterial geometry.

### **3. Modified Shortest Distance to the Outer Wall, Using Redistribution of Nodes**

In this method, we first segment the outer wall and the lumen at strategic points, where the curvature of the outer wall starts to change much more or less rapidly relative to that of the inner wall. Then, the outer wall nodes are redistributed so that each outer wall segment has the

number of nodes as the corresponding inner wall segment. For each segment, we then proceed as in the method 2.

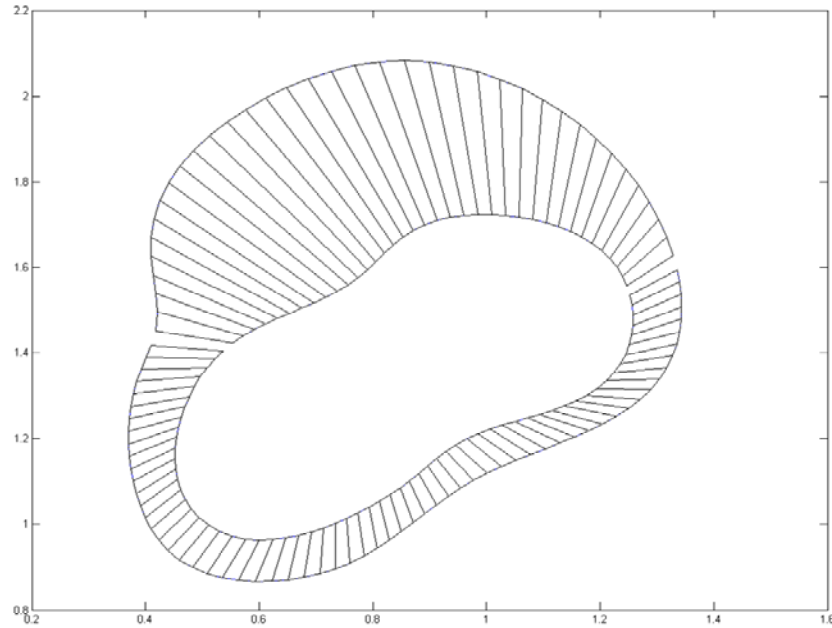


*Fig. 2.13 Shortest Distance to the Outer Wall, Using Redistribution of Nodes*

As done in this study, the arterial wall thickness increase is often taken as a useful indicator of plaque growth. (Kuhl et al., 2006). Therefore, in most studies concerning plaque in arteries, determining the wall thickness is a matter of immense importance. Therefore, this section would help to come up with a standardized and acceptable method of determining arterial wall thickness.

### 3. RESULTS FROM THE TWO-DIMENSIONAL MODELING APPROACH

This project used the distributions of the mechanical variables at the inner wall of the artery. For each two-dimensional transverse cross-section, 100 equi-spaced nodes were selected on the inner wall. The values of the mechanical variables of interest were obtained at these nodes from the corresponding finite element model. At each of these nodes, the wall thickness was determined using the modified shortest thickness approach described in section 2.3. The wall thickness was determined from the *in vivo* arterial contours, and not from the zero-stress arterial contours.

For each patient, the slices of the artery at the different time points were matched, and the wall thicknesses at the different time points were used to determine the Wall Thickness Increase (WTI) at each node as:

$$\text{WTI} = \text{Wall Thickness at time 2} - \text{Wall Thickness at time 1} \quad (3.1)$$

For each patient, we end up with a dataset containing the WTI and the mechanical variables.

### 3.1 Two Time-Point Analysis

For each patient, all matching internal carotid artery (ICA) slices from time 1 and time 2 were selected using the carotid bifurcation as the point of registration. For each patient, we have 300-700 data points depending on the number of matching ICA slices (100 points/slice). All data points for a given patient were treated equally (i.e., without reference to their locations).

**WTI vs.  $\sigma_{P1}$  at time 2** For each patient, the simple Pearson correlation between WTI from time 1 to time 2 and  $\sigma_{P1}$  at time 2 was quantified. Here, WTI approximates the plaque growth.  $\sigma_{P1}$ , the maximum principal value of the structural stress tensor, represents the structural stress. The linear least-squared regression between WTI and  $\sigma_{P1}$  at time 2 was quantified, and the corresponding daily plaque growth rate functions were obtained by dividing the regression coefficients by the time interval between time 1 and time 2. Table 3.1 summarizes the results for the 11 patients.

| Patient | Number of Data Points | Time Interval (days) | Daily Growth Rate (cm/day)<br>Unit for Stress: KPa | Pearson Coeff. |
|---------|-----------------------|----------------------|--|----------------|
| 1       | 500                   | 558                  | $9.337*10^{-05} - 1.633*10^{-06} \sigma_{P1}$      | -0.519**       |
| 2       | 300                   | 277                  | $2.363*10^{-04} - 4.513*10^{-06} \sigma_{P1}$      | -0.637**       |
| 3       | 400                   | 562                  | $2.875*10^{-04} - 5.000*10^{-06} \sigma_{P1}$      | -0.506**       |
| 4       | 600                   | 631                  | $-3.082*10^{-05} + 3.267*10^{-07} \sigma_{P1}$     | 0.0740         |
| 5       | 300                   | 520                  | $-1.557*10^{-04} + 2.654*10^{-06} \sigma_{P1}$     | 0.214          |
| 6       | 500                   | 1126                 | $7.465*10^{-05} - 8.059 *10^{-07} \sigma_{P1}$     | -0.566**       |
| 7       | 400                   | 298                  | $3.074*10^{-04} - 2.869*10^{-06} \sigma_{P1}$      | -0.298**       |
| 8       | 500                   | 495                  | $9.541*10^{-05} - 1.388*10^{-06} \sigma_{P1}$      | -0.315**       |
| 9       | 300                   | 549                  | $2.236*10^{-04} - 2.077*10^{-06} \sigma_{P1}$      | -0.369**       |
| 10      | 600                   | 461                  | $3.668*10^{-05} - 1.503*10^{-06} \sigma_{P1}$      | -0.361**       |
| 11      | 600                   | 525                  | $1.515*10^{-04} - 2.267*10^{-06} \sigma_{P1}$      | -0.399**       |

**Table 3.1 Plaque Progression (Wall Thickness Increase) vs. Maximum Principal Stress ( $\sigma_{P1}$ ) at Time 2,**  
\*\*p<0.0001

Therefore, significant correlation ( $p<0.0001$ ) was found between plaque growth, as estimated by wall thickness increase, and the structural  $\sigma_{P1}$  in 9 out of 11 patients. *This suggests that structural stress is indeed associated with plaque progression.*

Furthermore, the correlation between WTI and  $\sigma_{P1}$  at time 2 was found to be negative in 9 out of 11 patients. The 95% Confidence Interval for the Pearson Correlation coefficients for the 11 patients is [-0.510,-0.159]. This suggests that local thickening of arterial wall is associated with lowering of local  $\sigma_{P1}$  at the inner wall of the artery.

Please note that differentiating the inclusions from the normal arterial tissue does not seem to improve the correlations between WTI and  $\sigma_{P1}$  at time 2. For example, for patient 2, the

correlations for the three ICA slices are -0.769, -0.754 and -0.467 respectively if we differentiate the inclusions and are -0.789, -0.738, and -0.389 respectively if we do not differentiate the inclusions. Nonetheless, we would need to differentiate the inclusions from the normal arterial tissue in order to investigate the role of the fibrous cap and that of the variables inside the artery, such as at the boundary of the inclusions.

Also note that determining WTI by the shortest distance method gave the correlation for WTI vs.  $\sigma_{P1}$  to be -0.632 for patient 2, whereas using modified shortest distance method with  $\alpha=10$  degree gave a slightly better correlation of -0.637.

**WTI vs.  $\sigma_{P1}$  at time 1** WTI was found to be positively correlated with  $\sigma_{P1}$  at time 1 in 6 out of the 11 patients ( $p<0.001$ ) (see Table 3.2). The correlation was not significant at the  $\alpha=0.0001$  level in 4 patients, while it was significant negative in 1 patient. Therefore, the relation between WTI and  $\sigma_{P1}$  at time 1 is not particularly clear, though it does appear that there may be a positive correlation between WTI and  $\sigma_{P1}$  at time 1.

| Patient | PC (WTI vs. $\sigma_{P1}$ at time 1) |
|---------|--------------------------------------|
| 1       | -0.148                               |
| 2       | 0.324**                              |
| 3       | 0.547**                              |
| 4       | 0.524**                              |
| 5       | -0.0245                              |
| 6       | 0.0711                               |
| 7       | 0.408**                              |
| 8       | 0.0969                               |
| 9       | 0.234**                              |
| 10      | 0.602**                              |
| 11      | -0.304                               |

**Table 3.2 Correlation analysis results between WTI and  $\sigma_{P1}$  at Time 1. \*\* $p < 0.0001$ .**

It should be noted that the mechanical stress-induced plaque growth process simulated by Kuhl et al. (2006) also suggests that “pronounced growth takes place at the boundaries of the plaque in order to compensate local stress concentrations,” and that “high local stress concentrations can be observed at the plaque boundaries causing pronounced local growth in very small areas.”

**WTI vs. Other Structural Mechanical Variables** The simple Pearson correlation between WTI and certain other structural stress/ strain variables were quantified for each patient. Specifically, the correlation between WTI and the yz component  $\sigma_{yz}$  of the stress tensor, the yz component  $L_{yz}$  of the left stretch tensor, and the yz component  $R_{yz}$  of the right stretch tensor at time 1 and time 2 respectively were quantified. (The arterial cross-section is in the YZ plane). However,

consistently significant or strong correlations were not discovered. The results are summarized in Appendix D. These structural stress/ strain variables were other potential candidates to represent the structural contribution/ aspect of plaque progression. The lack of clear correlation between WTI and these variables suggest that these variables may not be important, at least directly, in the mechanism of plaque progression.

**WTI vs. Wall Thickness (WT)** WTI was found to be negatively correlated with WT at time 1 in 7 of the 11 patients, and positively correlated with WT at time 2 in 9 out of the 11 patients at the  $p < 0.0001$  level (see Table 3.3). The negatively correlation between WTI and WT at time 1 may mean that the wall thickens where the arterial wall is thin. Now, a thinner arterial wall generally corresponds to a higher  $\sigma_{P1}$  at the inner wall, and thickening of the arterial wall where it is thinner would tend to reduce the corresponding  $\sigma_{P1}$ . Therefore, this result is consistent with the hypothesis that the arterial wall thickens in areas of high  $\sigma_{P1}$ . The negative correlation between WTI and WT at time 2 may merely mean that thickening of the wall leads to increased WT.

To summarize the key findings reported in this section, the two time-point 2D analysis reveals that structural mechanics is indeed involved in the mechanism of plaque progression.  $\sigma_{P1}$  (which is the maximum principal value of the stress tensor) emerged as a leading candidate to represent the structural mechanics component in plaque progression. Plaque progression, estimated by Wall Thickness Increase (WTI), was found to be negatively correlated with the local  $\sigma_{P1}$  at the inner wall at time 2.

| PC (WTI vs. WT at time 1) | PC (WTI vs. WT at time 2) | Baseline Average WT (cm) |
|---------------------------|---------------------------|--------------------------|
| 0.128                     | 0.693                     | 0.148                    |
| -0.165                    | 0.895                     | 0.152                    |
| -0.492                    | -0.0803                   | 0.177                    |
| -0.540                    | -0.136                    | 0.215                    |
| 0.247                     | 0.666                     | 0.159                    |
| -0.629                    | 0.515                     | 0.131                    |
| -0.326                    | 0.633                     | 0.153                    |
| 0.0632                    | 0.505                     | 0.194                    |
| -0.129                    | 0.270                     | 0.157                    |
| -0.645                    | 0.309                     | 0.163                    |
| 0.237                     | 0.540                     | 0.190                    |

**Table 3.3 Correlation analysis results between WTI and WT at Time 1 and Time 2 respectively**

### 3.2 Three Time-Point Analysis

Utilizing data from three consecutive time points made it possible to explain a high percentage of the variability in the local WTI in terms of local structural stress, local wall thickness and plaque history.

The structural stress was represented by  $\sigma_{P1}$ , following the results of the previous section. Plaque history was represented by Wall Thickness Increase from time 1 to time 2 ( $WTI_{12}$ ).  $WTI_{23}$  was expressed in terms of  $\sigma_{P1}$  at time 2 ( $\sigma_{P12}$ ), wall thickness at time 2 ( $WT_2$ ) and the

corresponding  $WTI_{12}$ . Specifically,  $WTI_{23}$  was expressed as a linear combination of  $\sigma_{P12}$ ,  $WTI_{12} * \sigma_{P1}$ ,  $1/WT_2$ , and  $WTI_{12}/WT_2$ .

A slice-by-slice least-squared linear regression yielded high values of  $R^2$ , showing that a high percentage of the variability in  $WTI_{23}$  in each slice can be explained by taking the above four terms together. Table 3.4 presents the  $R^2$  values for each ICA slice for which matching data was available at 3 time points.

| Patient# | Slice 1 | Slice 2 | Slice 3 | Slice 4 | Slice 5 |
|----------|---------|---------|---------|---------|---------|
| 1        | 0.955   | 0.708   | 0.748   | 0.677   | 0.675   |
| 2        | 0.795   | 0.813   | X       | X       | X       |
| 3        | 0.906   | 0.836   | 0.954   | 0.916   | X       |
| 4        | X       | 0.459   | 0.868   | X       | 0.744   |
| 5        | 0.792   | 0.827   | 0.801   | X       | X       |
| 6        | 0.649   | 0.689   | 0.867   | 0.13    | 0.56    |
| 7        | 0.921   | 0.281   | 0.697   | 0.716   | X       |
| 8        | 0.967   | 0.833   | 0.939   | 0.863   | X       |
| 9        | 0.908   | 0.28    | 0.483   | 0.708   | X       |
| 10       | 0.683   | 0.663   | 0.584   | X       | X       |
| 11       | 0.767   | 0.291   | 0.432   | 0.719   | X       |

**Table 3.4 Coefficient of Determination  $R^2$  values for the OLS linear regression model to explain plaque progression in cross-sections of the Internal Carotid Artery (ICA). An “X” indicates corrupt time 3 data in the case of Patient# 4 and no matching slice at 3 time points for the other patients.**

For 35 out of the 42 slices,  $R^2$  exceeds 0.5, and is quite high in most of these slices. Therefore, local  $\sigma_{p1}$ , local wall thickness and plaque history together can consistently explain more than 50% of the variability in local WTI in a cross-section. Further, the expression picks up the trends in the WTI for several slices. Fig. 3.1 illustrates this for a randomly picked slice.

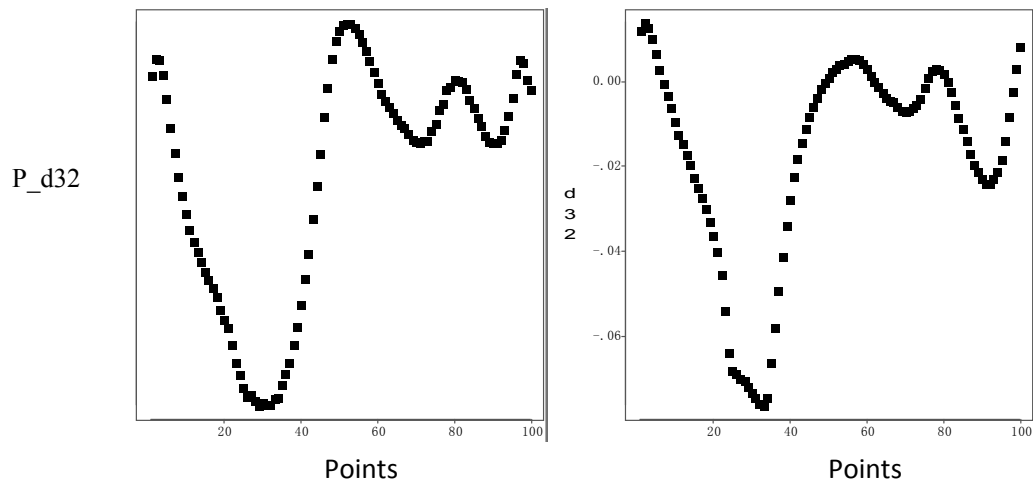


Fig. 3.1 Scatter plot of the predicted WTI ( $P_{d32}$ ) at 100 points on the inner wall of a slice vs. the scatter plot of actual WTI at the 100 points on the inner wall of the slice

**Remark 1: Rationale behind using  $WTI_{12}$  in the regression equation**

As mentioned in Chapter 1, atherosclerotic plaque growth is a multi-faceted process involving a number of different factors. Therefore, the variation in several factors from mechanical variables to biochemical variables around the inner wall may contribute to the variability in local WTI. Therefore, explaining a high percentage of this variability in local WTI using only mechanical variables may not be possible.

So, do we have any information regarding the relevant variables that are not in my dataset (such as variables pertaining to the biochemical condition in the artery)?

Yes, we do! The plaque history ( $WTI_{12}$ ) is the result of contribution from *all* factors involved in the plaque growth process from time 1 to time 2. Therefore,  $WTI_{12}$  contains information about all these factors, albeit at a higher level of abstraction. Therefore,  $WTI_{12}$  can be used to capture this information in explaining the variability in  $WTI_{13}$ .

**Remark 2**

Using information from three time points clearly allowed us to explain a higher percentage of the variability in WTI than was possible using information from only two time points. Therefore, our research approach of following the patients over several years, taking MRI scans for each patient at discrete time points, is justified.

Strictly speaking, in comparing the results from the two time points and three time points analysis, the adjusted  $R^2$  should be used to take into account the greater number of variables in the three time point result. However, the adjusted  $R^2$  values were found to differ from the corresponding  $R^2$  values by only 1 or 2 in the 2<sup>nd</sup> decimal place.

## **4. THREE-DIMENSIONAL MODELING APPROACH**

The two-dimensional modeling approach has two main limitations. First, we cannot simulate flow through a 2D transverse cross-section. Secondly, the two-dimensional models do not take into account the bonding between the arterial slices; each arterial slice that is modeled is modeled independently of its neighboring slices. A three-dimensional model would be free from these limitations. Therefore, the next step from the two-dimensional model is to model the artery at the three-dimensional level.

Reconstructing the 3D arterial geometry and making the 3D finite element mesh cannot be completely automated, and involve some manual work. It is time-consuming to both build the complete model and to process it. A good procedure would limit the error due to this human element and the time taken to build the model. Section 4.1 formalizes a computer-aided design approach to reconstructing the 3D arterial geometry. This approach deviates from previous approaches (by Prof. Tang's research group and others), and therefore, has been presented in some detail.

### **4.1 3D Geometry Reconstruction and Meshing**

The MRI-based 3D model geometry of the carotid artery was reconstructed using computer-aided design software SolidWorks (Copyright: SolidWorks Corporation). This section describes the procedure used to reconstruct the geometry.

The general procedure was to construct

Body<sub>w</sub>: a non-hollow 3D solid body whose external surface is defined by the wall boundary

Body<sub>l</sub>: a 3D solid body whose external surface is defined by the lumen boundary

Then, the geometric model for the artery was obtained as (Body<sub>w</sub> - Body<sub>l</sub>)

This is next described in detail, and illustrated using the specific case of the patient Y3.

#### 4.1.1 Constructing Body<sub>w</sub>

I started out with the discrete sampling of the external wall at transverse cross-sections of the artery at regular spacing of 2mm.

For each slice, the contour of the external wall was constructed by joining its points using cubic spline interpolation. This step is similar to what was done for the 2D geometry reconstruction. The curvature of the spline is continuous at the control points. Fig. 4.1 shows the contours for the external wall of the artery of a patient.

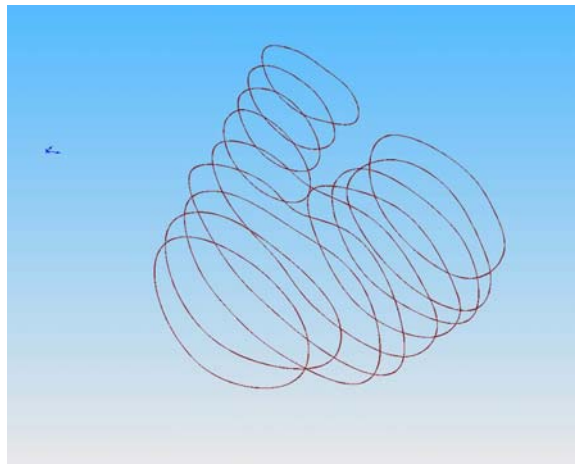


*Fig. 4.1 External wall contours of the arterial slices of the patient Y3 reconstructed using segmented MRI data and spline interpolation*

Body<sub>w</sub> was next constructed in five separate parts:

- i) The common part of the carotid artery (CCA)
- ii) The internal branch of the carotid artery (ICA) proximal to the bifurcation
- iii) The external branch of the carotid artery (ECA) proximal to the bifurcation
- iv) The internal branch of the carotid artery (ICA\*) distal to the bifurcation
- v) The external branch of the carotid artery (ECA\*) distal to the bifurcation

- i) CCA was constructed from the parallel contours of the external wall up to the bifurcation slice. Fig. 4.2 explicitly shows these contours.

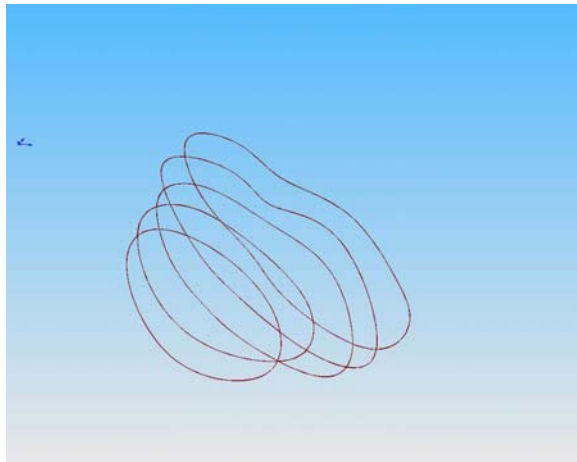


*Fig. 4.2 Contours used to construct the external wall of the common carotid artery (CCA)*

The corresponding solid body was generated using longitudinal splines (Barratt et al., 2004). SolidWork's Lofted Boss/ Base feature was used to do this. For each of these contours, the "first" point was manually selected such that the "first" points of the contours were matched. This selection of the "first points" was the human element in this step. The choice of the "first points" was motivated by resemblance between the contours, and was also aimed at minimizing internal twists in the geometry. Fig. 4.3 shows the corresponding solid geometry of the CCA.

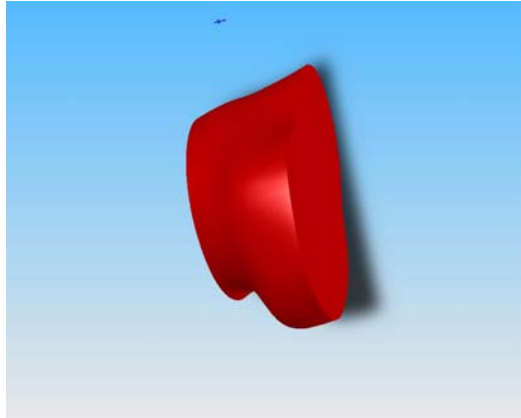


*Fig. 4.3 Solid geometry of the common carotid artery (CCA) of the patient Y3 in SolidWorks*

- ii) The internal branch of the carotid artery proximal to the bifurcation (ICA) was constructed from the two contours labeled **a** and **b** in fig. 4.4 below.

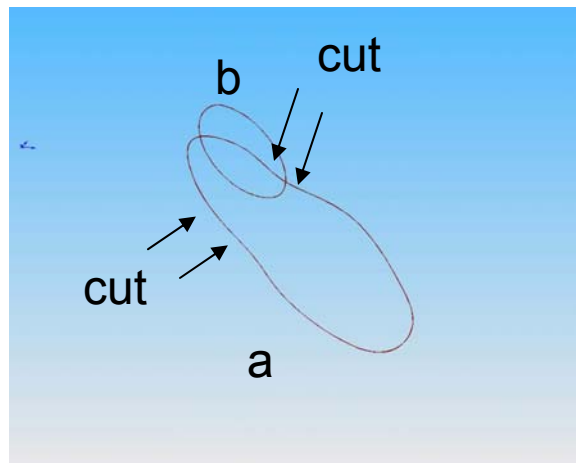


*Fig. 4.4 Contours used to construct the ICA proximal to the bifurcation*

To do this, the contour labeled **a** was first cut at four points near the region where it begins to bifurcate, roughly shown in fig. 4.4 by use of arrows. The two open endpoints of the left-most piece in fig. 4.4 were next joined by a cubic spline to form a closed loop. The curvature of the spline is continuous at the end-points. Let this closed loop be named **a1**.

Choosing the points at which the curve **a** is cut represents the 2<sup>nd</sup> and final human element in this construction procedure.

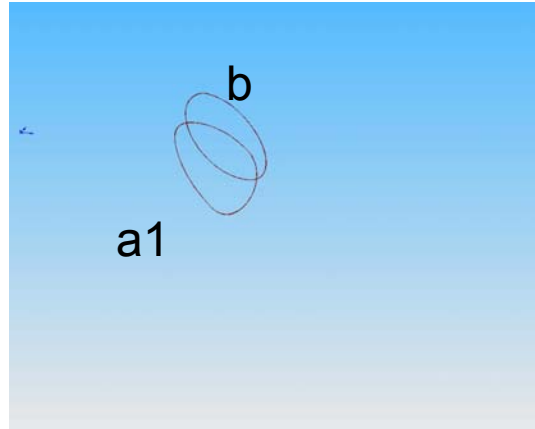


*Fig. 4.5 Curves a1 and b used to construct the ICA proximal to the bifurcation*

SolidWork's Lofted Boss/ Base feature was used to construct the solid between curves **a1** and **b**. This solid piece models the branching off of the artery into the internal carotid artery.

- iii) The external branch of the carotid artery proximal to the bifurcation (ECA) was modeled in the same way as ICA, but using the rightmost piece instead of **a1** in fig. 4.4.
- iv) The internal branch of the carotid artery distal to the bifurcation (ICA\*) was modeled using the corresponding contours from curve **b** onwards. Fig. 4.6 shows the curves used.

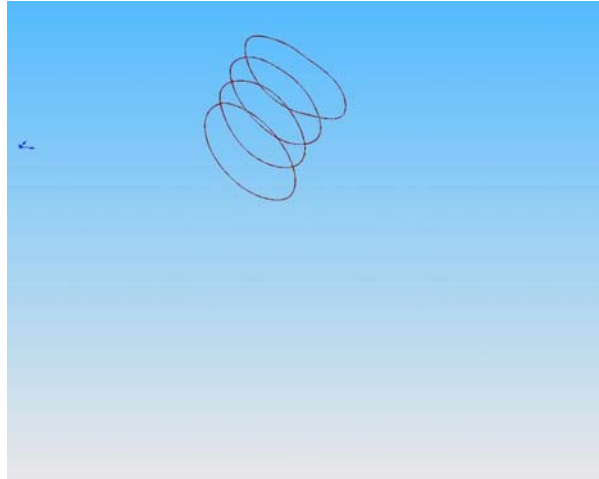


*Fig. 4.6 Contours used to construct the ICA distal to the bifurcation (ICA\*)*

- v) The ECA distal to the bifurcation (ECA\*) was modeled using the corresponding contours shown in fig. 4.7.

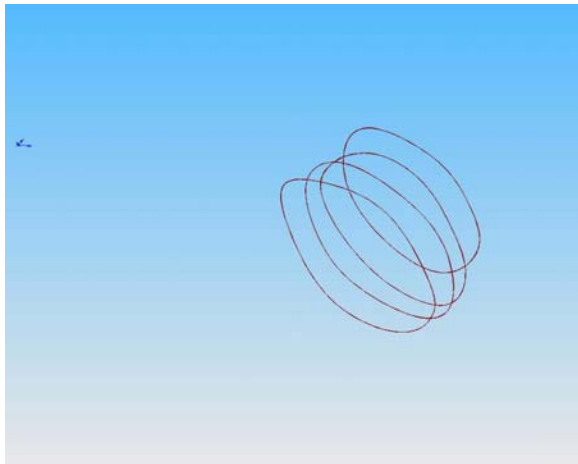


*Fig. 4.7 Contours used to construct ECA distal to the bifurcation (ECA\*)*

These five body parts were imported into Adina as parasolid bodies. (Parasolid body is a type of file format for bodies that is supported by several CAD softwares). In Adina, these five bodies were merged together using its boolean function into a single body: Body<sub>w</sub>.



*Fig. 4.8 Image of Body<sub>w</sub>.*

#### **4.1.2 Constructing Body<sub>l</sub>**

Body<sub>l</sub> was constructed in the same way as Body<sub>w</sub>, but using the lumen wall contours instead of the outer wall contours.

#### **4.1.3 Constructing the Body of the Artery**

The solid part of the artery was constructed by subtracting body<sub>l</sub> from body<sub>w</sub> using a boolean function in Adina. The solid body could now be meshed (unstructured triangulated) in Adina. Fig. 4.9 presents such a mesh. It may be necessary to create a finer mesh in certain localized areas.

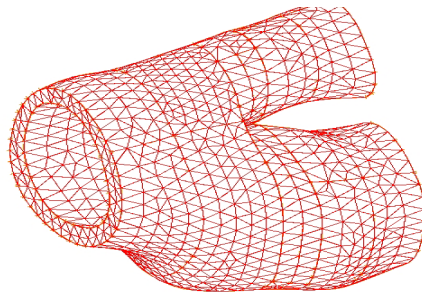


*Fig. 4.9 Geometry and Mesh of a carotid artery*

The flow-only model and the FSI model would simulate *streamlined* blood flow through this section of the artery. To achieve this, a 10 cm length of artery is added to the base; when the blood is injected at the appropriate pressure into the artery, it would have achieved its streamlined profile by the time it reaches the section of the artery that we are interested in.

A length of 6 cm of artery each is also added to the ICA and the ECA respectively in order to extend them by 6 cm each. This ensures that the flowing blood would not introduce spurious end effects in the section of the artery we are interested in.

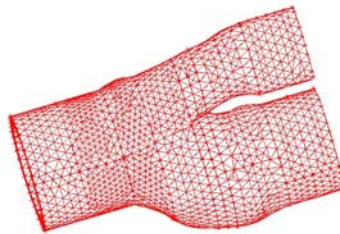


*Fig. 4.10 Geometry and mesh of the extended artery*

## 4.2 Solid-Only Model

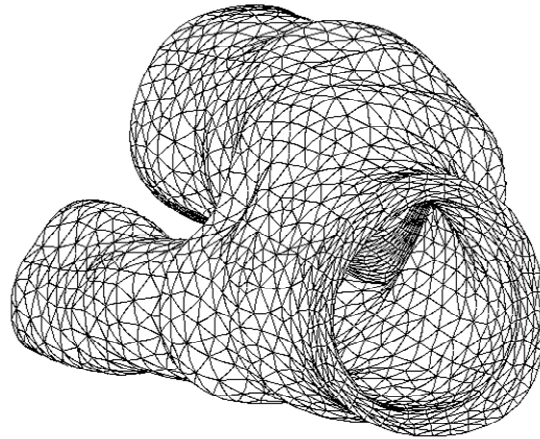


*Fig. 4.11 Mesh for the Solid-only Model*

The solid-only model was processed in the finite element software Adina with the following loadings:

1. A normal, outward directed pressure applied to the lumen boundary. The magnitude of the pressure is chosen to be the systolic blood pressure of the specific patient. This load simulates the normal blood pressure on the arterial material.
2. Displacements applied at the three open faces of the artery. The artery in the body is held by attachments to the body, and this stretches the artery and holds it in place. This axial stretch aims to simulate this condition.

Fig. 4.12a presents the band-plots of the displacement magnitudes obtained from the processed solid-only model, and fig. 4.12b presents that obtained from a processed model with cylindrical geometry and under similar loading, for comparison with fig. 4.12a.

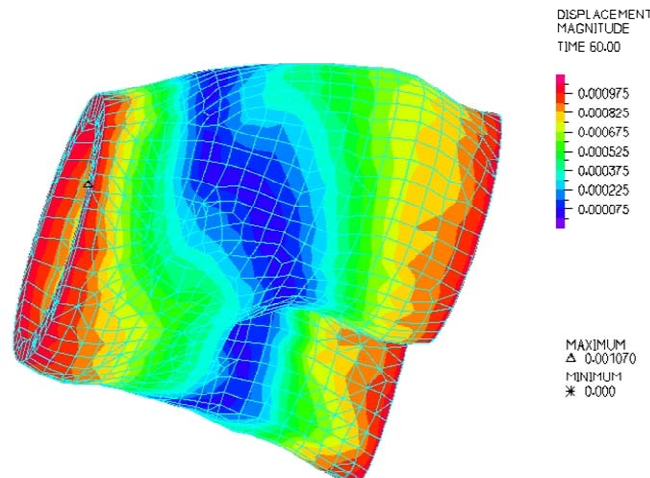


*Fig. 4.12a Band-plot of the displacement magnitude in the artery obtained from the processed solid-only model*

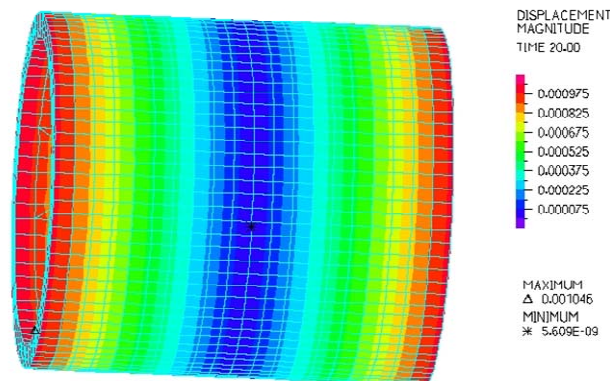


*Fig. 4.12b Band-plot of the displacement magnitude obtained from a processed model with cylindrical geometry and loading similar to that imposed on the artery*

### 4.3 Flow-Only Model

Body<sub>1</sub> (see section 4.1.2) was used for the geometry of the flow-only model. The model was processed with a physiological inlet and outlet pressure (Beattie, Vito et al.). The pressure difference between the inlet and the outlet drives the blood flow in the model.

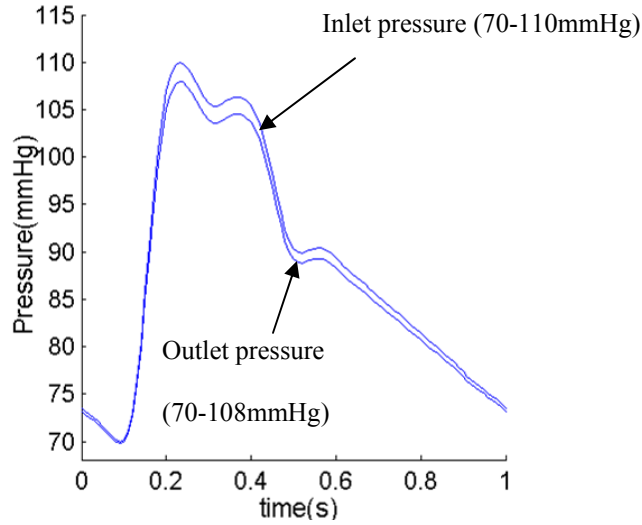


Fig. 4.13 Pressure imposed at the inlet and outlet of the artery

Fig. 4.14 displays the obtained velocity field on a longitudinal cut in the artery.

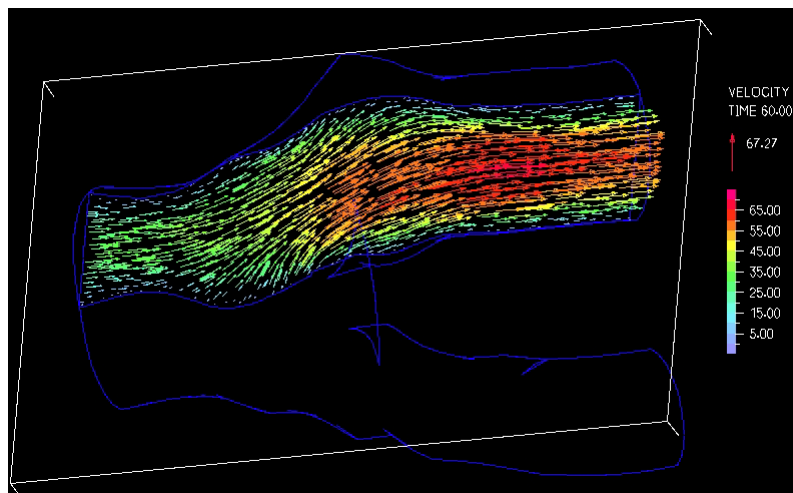


Fig. 4.14 Velocity field displayed on a longitudinal cut in the artery. Velocity magnitudes are in units of cm/s

#### 4.4 Results from the three-dimensional modeling approach<sup>1</sup>

Fig. 4.15 gives plots of wall thickness increase (WTI) vs. inner wall  $\sigma_{P_1}$  at time 2 and wall Maximum Shear Stress ( $\tau$ ) at time 1, using results from a 3D FSI model (240 data points from 6 slices, time interval: 304 days).

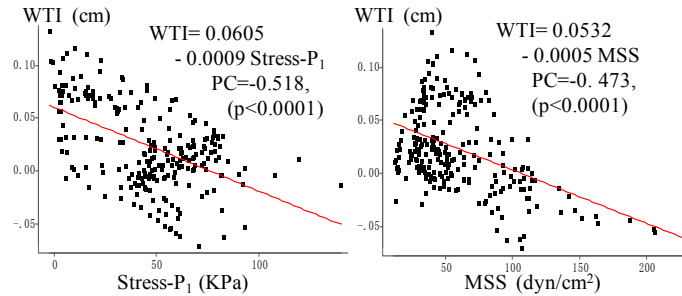


Fig. 4.15 Wall Thickness increase (WTI) vs. structure  $\sigma_{P_1}$  and wall flow Maximum Shear Stress (MSS)

The linear approximations for WTI given by the least squares linear regression are:

$$\text{WTI} = 0.0605 - 0.000790 \sigma, \quad (\text{PC} = -0.518, R^2 = 0.268, p < 0.0001), \quad (4.1)$$

$$\text{WTI} = 0.0532 - 0.000507 \tau, \quad (\text{PC} = -0.473, R^2 = 0.224, p < 0.0001), \quad (4.2)$$

$$\text{WTI} = 0.1307 - 0.000936 \sigma - 0.000616 \tau, \quad (R^2 = 0.589). \quad (4.3)$$

The plaque daily growth rate (daily WTI) is given by:

---

<sup>1</sup> Sayan Mondal, Chun Yang, Joseph D. Petrucci, Chun Yuan, Fei Liu, Tom Hatsukami, Dalin Tang, “A New Hypothesis for Human Atherosclerotic Plaque Progression based on Serial In Vivo MRI and Computational Modeling Method”, ASME 2007 Summer Bioengineering Conference.

$$dWTI=0.00043-3.08 e^{-6} \sigma - 2.026 10^{-6} \tau. \quad (4.4)$$

Using only the 5 ICA slices (200 points), we have better correlations:

$$WTI= 0.0637 - 0.000897 \sigma, (PC=-0.528, R^2=0.279), \quad (4.5)$$

$$WTI= 0.0619 - 0.000578 \tau, (PC=-0.525, R^2=0.276), \quad (4.6)$$

$$WTI=0.112 - 0.00103 \sigma - 0.000663 \tau, (R^2=0.637). \quad (4.7)$$

Therefore, we find negative correlation between WTI and  $\sigma_{P1}$  at time 2, in agreement with results presented in Chapter 3. We also find negative correlation between WTI and MSS at time 1, in agreement with previous research studies (Ku, 1997). Taken together, the two variables explain a higher percentage of the variability in local WTI than each does individually (compare the  $R^2$  between Eqs. 4.5, 4.6 and 4.7).

## 5. SIGNIFICANCE AND FUTURE DIRECTIONS

This project used patient-specific *in vivo* MRI-based computational modeling to provide insights into the mechanism of atherosclerotic plaque growth. Overall, this work documented quantitative data showing correlation between carotid atherosclerotic plaque progression and structural stress. To our knowledge, we are the first group to report such research results.

This project has made several contributions to the research on atherosclerotic plaque progression.

It has developed and implemented a shrinking procedure to reconstruct the zero-stress state of the artery for two-dimensional modeling. The two-dimensional models in this project are some of the first to apply the loadings to the zero-stress geometry of the artery, and not directly to the arterial geometry observed in the MRI. Furthermore, the shrinking procedure developed in the course of this project is the first to respect the law of mass conservation.

It has explicitly formulated plausible procedures to determine arterial wall thickness, and has suggested a method to determine the arterial wall thickness at cross-sections having particularly irregular geometry.

It has developed a computer-aided design procedure to reconstruct the three-dimensional geometry of the artery that seeks to minimize and localize the human element in the reconstruction and meshing process. This is a step towards automating the three-dimensional modeling of artery— something that would be quite desirable but yet to be achieved.

Structural stress was identified to be involved in the mechanism of atherosclerotic plaque growth.  $\sigma_{P1}$  emerged as a leading candidate to represent structural stress in the process of plaque growth.

The correlations and ordinary least-squared linear regressions between plaque growth and structural stresses were quantified and documented for the first time.

A dependence of plaque growth on local structural stress, arterial wall thickness and plaque history was discovered. This dependence consistently explained a high percentage of the variability in plaque progression in the arterial cross-sections for which we have MRI data

Atherosclerotic plaque growth and rupture in carotid arteries often result in stroke— a leading cause of death in the developed world. Several research teams (e.g., Humphrey et al., 2003; Karniadakis et al., 2006; Ku et al., 1997; Kuhl et al., 2006; Tang et al., 2007) are currently engaged in investigating issues related to atherosclerotic plaque growth and rupture. The discoveries documented in this project and in papers published in the course of this project have contributed to the ongoing efforts in stroke research. Results from this project may also motivate a similar investigation into plaque growth in coronary arteries— a leading cause of heart attack.

This project was supported in part by the NSF grant DMS-0540684, and is a part of a 5-year project to investigate the mechanism of atherosclerotic plaque growth, determine risk factors for plaque rupture, and assess plaque vulnerability. Next, more patient-based three-dimensional computational models would be constructed, and corresponding datasets analyzed based on the results of this project. In the context of three-dimensional modeling, mesh-free methods such as the Petrov-Galerkin method may be used to save the meshing-remeshing costs

due to the large deformations of artery. The plaque growth functions quantified in this project may be used to simulate plaque growth in humans, and make patient-specific predictions.

## Bibliography

1. American Heart Association. *Heart Disease and Stroke Statistics – 2007 Update*. Dallas, Tex. American Heart Association; 2007.
2. Barratt CD, Ariff BB, Humphries KN, Thom SA, Hughes AD. Reconstruction and Quantification of the Carotid Artery Bifurcation from 3-D Ultrasound Images. *IEEE Transactions on Medical Imaging*, 23:567-583, 2004.
3. Bathe KJ. Theory and Modeling Guide, Vol I: ADINA; Vol II: ADINA-F, ADINA R&D, Inc., Watertown, MA, 2002.
4. Berlinger JA, Navab M, Fogelman AM, Frank JS, Demer LL, Edwards PA, Watson AD, Lusis AJ. Atherosclerosis: Basic Mechanisms Oxidation, Inflammation and Genetics. *Circulation*. 91:2488-2496, 1995.
5. Dong S, Insley J, Karonis NT, Papka M, Binns J, Karniadakis GE. Simulating and visualizing the human arterial system on the TeraGrid. *The International Journal of Grid Computing: Theory, Methods and Applications*. 22:1011-1017, 2006.
6. Friedman MH. Arteriosclerosis research Using vascular flow models: From 2-D branches to compliant replicas. *J. Biomech. Engng*. 115:595-601, 1993.
7. Giddens DP, Zarins CK, Glagov S. The role of fluid mechanics in the localization and detection of atherosclerosis. *J. Biomech. Engng*. 115:588-594, 1993.
8. Huang H, Virmani R, Younis H, Burke AP, Kamm RD, Lee RT. The impact of calcification on the biomechanical stability of atherosclerotic plaques. *Circulation*, 103: 1051-1056, 2001.

9. Humphrey JD, Rajagopal KR (2002). A constrained mixture model for growth and remodeling of soft tissues. *Math Models Methods Appl. Sci.* 12:407-430.
10. Humphrey JD, Rajagopal KR (2003). A Constrained mixture model for arterial adaptations to a sustained step change in blood flow. *J. Biomech Model Mechanobiology.* 109-126
11. Indolfi C. Genetic factors in atherosclerosis: status and perspectives. *European Heart Journal Supplements.* Supplement B, B14-B16.
12. Ku DN. Blood Flow in Arteries. *Annual Review of Fluid Mechanics.* 29: 399-434, 1997.
13. Ku DN, Giddens DP, Zarins CK, Glagov S. Pulsatile flow and atherosclerosis in the human carotid bifurcation: positive correlation between plaque location and low and oscillating shear stress. *Arteriosclerosis.* 5:293-302, 1985.
14. Kuhl E, Maas R, Himpel G, Menzel R. Computational modeling of arterial wall growth: Attempts towards patient-specific simulations based on computer tomography. *J. Biomechanics and Modeling in Mechanobiology.* 6: 321-331, 2007.
15. Mondal S, Yang C, Petruccelli JD, Yuan C, Liu F, Hatsukami T, Tang D. 3D multi-component FSI models based on multi-year *in vivo* MR images for human atherosclerotic plaque progression investigation. *Compilation of Abstracts for the Fourth M.I.T. Conference on Computational Fluid and Solid Mechanics*, Boston, MA, 2007, pp. 28.
16. Mondal S, Yang C, Petruccelli JD, Yuan C, Liu F, Hatsukami T, Tang D. A New Hypothesis for Human Atherosclerotic Plaque Progression Based on Serial *In Vivo* MRI and Computational Modeling Method, *Proceedings of the 2007 ASME Summer Bioengineering Conference*, Keystone, CO, 2007, Abstract# SBC2007-175504.
17. Naghavi M, Libby P, Falk E, Casscells SW, Litovsky S, Rumberger J, Badimon JJ, Stefanadis C, Moreno P, Pasterkamp G, Fayad Z, Stone PH, Waxman S, Raggi P, Madjid M,

- Zarrabi A, Burke A, Yuan C, Fitzgerald PJ, Siscovick DS, de Korte CL, Aikawa M, Juhani Airaksinen KE, Assmann G, Becker CR, Chesebro JH, Farb A, Galis ZS, Jackson C, Jang IK, Koenig W, Lodder RA, March K, Demirovic J, Navab M, Priori SG, Rekhter MD, Bahr R, Grundy SM, Mehran R, Colombo A, Boerwinkle E, Ballantyne C, Insull W Jr, Schwartz RS, Vogel R, Serruys PW, Hansson GK, Faxon DP, Kaul S, Drexler H, Greenland P, Muller JE, Virmani R, Ridker PM, Zipes DP, Shah PK, Willerson JT. From vulnerable plaque to vulnerable patient: a call for new definitions and risk assessment strategies: Part I. *Circulation*. 108(14):1664-72, 2003.
18. Naghavi M, (same as above). From vulnerable plaque to vulnerable patient: a call for new definitions and risk assessment strategies: Part II. *Circulation*. 108(15):1772-8, 2003.
19. Ravn HB, Falk E. Histopathology of plaque rupture. *Cardiology clinics*. 17:263-270, 1999.
20. Steinman DA, Thomas JB, Ladak HM, Milner JS, Rutt BK, Spence JD. Reconstruction of Carotid Bifurcation Hemodynamics and Wall Thickness Using Computational Fluid Dynamics and MRI. *Magnetic Resonance in Medicine* 47:149-159, 2002.
21. Tang D, Yang C, Zheng J, Woodard PK, Sicard GA, Saffitz JE, Yuan C. 3D MRI-based multi-component FSI models for atherosclerotic plaques, a 3-D FSI Model. *Annals of Biomedical Engineering*, 32(7):947-960.
22. Tang D, Yang C, Petrucci JD, Yuan C, Liu F, Hatsukami T, Mondal S, Atluri S. Quantifying Human Atherosclerotic Plaque Growth Function Using Multi-Year *In Vivo* MRI and Meshless Local Petrov-Galerkin Method. *Proceedings: 2007 IEEE/ICME International Conference on Complex Medical Engineering*, Beijing, China, 2007, pp. 541-546.

23. Tang D, Yang C, Mondal S, Liu F, Canton G, Hatsukami T, Yuan C. A Negative Correlation between Human Carotid Atherosclerotic Plaque Progression and Plaque Wall Stress: *In Vivo* MRI-Based 2D/ 3D FSI Models, to appear in the *Journal of Biomechanics*.
24. Underhill HR, Kerwin WS, Hatsukami TS, Yuan C. Automated Measurement of Mean Wall Thickness in the Common Carotid Artery by MRI: A Comparison to Intima-Media Thickness by B-Mode Ultrasound. *J. Magnetic Resonance Imaging* 24:379–387, 2006.
25. Yuan C, Kerwin WS, Ferguson MS, Polissar N, Zhang SX, Cai JM, Hatsukami TS. Contrast enhanced high resolution MRI for atherosclerotic carotid artery tissue characterization. *JMRI*, 15:62-67, 2002.

# APPENDICES

## A. Matlab Code to Implement the Shrinking Procedure

```
clear
%%%%%%%%%%%%%%%%%%%%%%%%%%%%%%%%%%%%%%%%%%%%%%%%%%%%%%%%%%%%%%%%%%%%%%%%SHRINKING WITH AREA CONSERVATION%%%%%%%%%%%%%%%%%%%%%%%%%%%%%%%%%%%%%%%%%%%%%%%%%%%%%%%%%%%%%%%%%%%%%%%%
%%%%%%%%%%%%%%%%%%%%%%%%%%%%%%%%%%%%%%%%%%%%%%%%%%%%%%%%%%%%%%%%%%%%%%%%Sayan Mondal%%%%%%%%%%%%%%%%%%%%%%%%%%%%%%%%%%%%%%%%%%%%%%%%%%%%%%%%%%%%%%%%%%%%%%%%
%%%%%%%%%%%%%%%%%%%%%%%%%%%%%%%%%%%%%%%%%%%%%%%%%%%%%%%%%%%%%%%%%%%%%%%%Matlab code, 2007 Edition%%%%%%%%%%%%%%%%%%%%%%%%%%%%%%%%%%%%%%%%%%%%%%%%%%%%%%%%%%%%%%%%%%%%%%%%
%%%%%%%%%%%%%%%%%%%%%%%%%%%%%%%%%%%%%%%%%%%%%%%%%%%%%%%%%%%%%%%%%%%%%%%%
%%%%%%%%%%%%%%%%%%%%%%%%%%%%%%%%%%%%%%%%%%%%%%%%%%%%%%%%%%%%%%%%%%%%%%%%INPUT%%%%%%%%%%%%%%%%%%%%%%%%%%%%%%%%%%%%%%%%%%%%%%%%%%%%%%%%%%%%%%%%%%%%%%%%Number of points in each contour-----
shrink= ; %shrunk lumen=shrink*original lumen. shrink<1
l= ; %number of points given for the lumen
w= ; %number of points given for the wall
i1= ; %number of points given for inclusion#1. Enter 0 if no inclusion.
i2=0;
i3=0;
%%%%%%%%%%%%%%%%%%%%%%%%%%%%%%%%%%%%%%%%%%%%%%%%%%%%%%%%%%%%%%%%%%%%%%%%Copies data into matrices-----
f1=fopen('lumen.txt','rt+') ; %lumen.txt contains the lumen coordinates in
pixels
lumen=fscanf(f1,'%e',[2,l]);
fclose(f1);
f2=fopen('wall.txt','rt+') ;
wall=fscanf(f2,'%e',[2,w]);
fclose(f2);
% f4=fopen('inclusion2.txt','rt+'); % If there is an inclusion, use this
% part of the code.
% incl2=fscanf(f4,'%e',[2,i2]);
% fclose(f4);
% f5=fopen('inclusion3.txt','rt+');
% incl3=fscanf(f5,'%e',[2,i3]);
% fclose(f5);
%%%%%%%%%%%%%%%%%%%%%%%%%%%%%%%%%%%%%%%%%%%%%%%%%%%%%%%%%%%%%%%%%%%%%%%%Converts the data from pix to cm, and stores in vectors---
xlumen=0.03125*lumen(1,:);
ylumen=0.03125*lumen(2,:);
xwall=0.03125*wall(1,:);
ywall=0.03125*wall(2,:);
%%%%%%%%%%%%%%%%%%%%%%%%%%%%%%%%%%%%%%%%%%%%%%%%%%%%%%%%%%%%%%%%%%%%%%%%
arealumen=0.5*(trapz(xlumen,ylumen)-trapz(ylumen,xlumen)); %determines area
%enclosed in the closed loop of the lumen using area formula derived from
%Green's theorem.
areawall=0.5*(trapz(xwall,ywall)-trapz(ywall,xwall));
area=abs(areawall)-abs(arealumen); %computes the area of the original slice
%%%%%%%%%%%%%%%%%%%%%%%%%%%%%%%%%%%%%%%%%%%%%%%%%%%%%%%%%%%%%%%%%%%%%%%%Determines the Centroid of the Original Wall---
gw=xwall.*xwall;
fw=ywall.*ywall;
centroidXw=0.5*trapz(gw,ywall)/areawall;
centroidYw=-0.5*trapz(fw,xwall)/areawall;
%%%%%%%%%%%%%%%%%%%%%%%%%%%%%%%%%%%%%%%%%%%%%%%%%%%%%%%%%%%%%%%%%%%%%%%%
%%%%%%%%%%%%%%%%%%%%%%%%%%%%%%%%%%%%%%%%%%%%%%%%%%%%%%%%%%%%%%%%%%%%%%%%Determines the Centroid of the Original Lumen
gl=xlumen.*xlumen;
```

```

fl=ylumen.*ylumen;
centroidXl=0.5*trapz(gl,ylumen)/arealumen;
centroidYl=-0.5*trapz(fl,xlumen)/arealumen;
%%%%%%%%%%%%%%%%%%%%%%%%%%%%%%%%%%%%%%%%%%%%%%%%%%%%%%%%%%%%%%%%%%%%%%%%
xlumenshrunk=shrink*xlumen; %computes coordinates of the shrunk lumen
ylumenshrunk=shrink*ylumen;
arealumenshrunk=0.5*(trapz(xlumenshrunk,ylumenshrunk)-
trapz(ylumenshrunk,xlumenshrunk));
%%%%%%%%%%%%%%%%%%%%%%%%%%%%%%%%%%%%%%%%%%%%%%%%%%%%%%%%%%%%%%%%%%%%%%%%Determines the Centroid of the Shrunk Lumen%%%
gls=xlumenshrunk.*xlumenshrunk;
fls=ylumenshrunk.*ylumenshrunk;
centroidXlumenshrunk=0.5*trapz(gls,ylumenshrunk)/arealumenshrunk;
centroidYlumenshrunk=-0.5*trapz(fl,xlumenshrunk)/arealumenshrunk;
%%%%%%%%%%%%%%%%%%%%%%%%%%%%%%%%%%%%%%%%%%%%%%%%%%%%%%%%%%%%%%%%%%%%%%%%
areashrunk=abs(areawall)-abs(arealumenshrunk); %this is the area of the
%slice with the lumen shrunk but wall not shrunk
b=1 %b initializes the shrinkage of the wall. starting shrunk wall=b*original
wall
%this loop evaluates b, such that the area of the shrunk slice is conserved
%within 1%.
for i=1:1000
xwallb=b*xwall;
ywallb=b*ywall;
areawallb=0.5*(trapz(xwallb,ywallb)-trapz(ywallb,xwallb));
areab=abs(areawallb)-abs(arealumenshrunk);
a=100*(areab-area)/area; %a is the percentage discrepancy between area of
shrunk slice and original slice.
if a>1
    b=b-0.005;
end
if a<-1
    b=b+0.005;
end
end
%%%%%%%%%%%%%%%%%%%%%%%%%%%%%%%%%%%%%%%%%%%%%%%%%%%%%%%%%%%%%%%%%%%%%%%%Determines the centroid of the shrunk Wall%%%%%%%%
gws=xwallb.*xwallb;
fws=ywallb.*ywallb;
centroidXwallshrunk=0.5*trapz(gws,ywallb)/(areawallb);
centroidYwallshrunk=-0.5*trapz(fws,xwallb)/(areawallb);
%%%%%%%%%%%%%%%%%%%%%%%%%%%%%%%%%%%%%%%%%%%%%%%%%%%%%%%%%%%%%%%%%%%%%%%%
%%%%%%%%On Shrinking, How much did the centroids get displaced by ?%%%%%%%%
dxwall=abs(centroidXw)-abs(centroidXwallshrunk);
dywall=abs(centroidYw)-abs(centroidYwallshrunk);
dxlumen=abs(centroidXl)-abs(centroidXlumenshrunk);
dylumen=abs(centroidYl)-abs(centroidYlumenshrunk);
xwallfinal=xwallb + dxwall;
ywallfinal=ywallb + dywall;
xlumenfinal=xlumenshrunk + dxlumen;
ylumenfinal=ylumenshrunk + dylumen;
%%%%%%%%%%%%%%%%%%%%%%%%%%%%%%%%%%%%%%%%%%%%%%%%%%%%%%%%%%%%%%%%%%%%%%%%Plot%%%%%%%%
figure
plot(xlumenfinal,ylumenfinal,'k');
hold on
plot(xlumen,ylumen);
hold on
plot(xwallfinal,ywallfinal,'k')
hold on

```

```

plot(xwall,ywall)
%%%%%%%%%%%%%%%%%%%%%%%%%%%%%%%%%%%%%%%%%%%%%%%%%%%%%%%%%%%%%%%%%%%%%%%%Puts coordinates into appropriate form%%%%%%%%%%%%%%%%%%%%%%%%%%%%%%%%%%%%%%%%%%%%%%%%%%%%%%%%%%%%%%%%%%%%%%%%
xwallfinalt=xwallfinal';
ywallfinalt=ywallfinal';
xlumenfinalt=xlumenfinal';
ylumenfinalt=ylumenfinal';
zl=zeros(1,1);
zw=zeros(w,1);
wallcoord=horzcat(zw,xwallfinalt,ywallfinalt);
lumencoord=horzcat(zl,xlumenfinalt,ylumenfinalt);
coord=vertcat(wallcoord,lumencoord);
%%%%%%%%%%%%%%%%%%%%%%%%%%%%%%%%%%%%%%%%%%%%%%%%%%%%%%%%%%%%%%%%%%%%%%%%Tackles inclusion#1%%%%%%%%%%%%%%%%%%%%%%%%%%%%%%%%%%%%%%%%%%%%%%%%%%%%%%%%%%%%%%%%%%%%%%%%
f3=fopen('inclusion1.txt','rt+');
incl1=fscanf(f3,'%e',[2,i1]);
fclose(f3);
xinclusion1=0.03125*incl1(1,:); %converts pixel to cm, and stores the data in
vectors
yinclusion1=0.03125*incl1(2,:);
areainclusion1=abs(0.5*(trapz(xinclusion1,yinclusion1)-
trapz(yinclusion1,xinclusion1)));
%%Converts to polar coordinates, center at the centroid of the lumen
[alpha,r]=cart2pol(xinclusion1-centroidXl,yinclusion1-centroidYl);
%%Determines the "extreme points" of the inclusion, preliminary to
%%splitting the inclusion
% for ss=1:i1
%     if(alpha(ss)<0)
%         alpha(ss)=alpha(ss)+2*pi;
%     end
% end
for ss=1:(i1-1)
dalpha(ss)=alpha(ss+1)-alpha(ss);
end
n=0;
for mm=1:(i1-2)
if(sign(dalpha(mm))~=sign(dalpha(mm+1)))
    n=n+1;
point(n)=mm;
end
end
% [amax,point_max]=max(abs(alpha));
% [amin,point_min]=min(abs(alpha));
% N=min(point_max,point_min);
% M=max(point_max,point_min);
e='ERROR ERROR ERROR ERROR ERROR';
if(length(point)==2)
N=min(point)
M=max(point)
else
    e
    N=max(point);
    M=length(i1);
end
%%
d=1;%initializes d that will eventually control the position of the part of
the inclusion nearer the lumen
abc(1,1)=1; % abc(:,1) is cosmetic, has no impact.
abc(2,1)=N;

```

```

abc(3,1)=M;
%%%Next, which part of the inclusion is to be shrunk using b and which to
%%%be shrunk using d? The inclusion contour has three parts [1,N],[N+1,M],
%%[M+1, end point i1] and we associate either bdb or dbd with these three
%%parts respectively.
if(r(N+4)<r(5))
    abc(1,2)=d;
    abc(2,2)=b;
    abc(3,2)=d;
    ab(1)='d';
    ab(2)='b';
    ab(3)='d';
end
if(r(N+4)>r(5))
    abc(1,2)=b;
    abc(2,2)=d;
    abc(3,2)=b;
    ab(1)='b';
    ab(2)='d';
    ab(3)='b';
end
if(N==1)
    if(r(N+4)<r(i1-4))
        abc(1,2)=d;
        abc(2,2)=shrink;
        abc(3,2)=d;
        ab(1)='d';
        ab(2)='b';
        ab(3)='d';
    end
    if(r(N+4)>r(i1-4))
        abc(1,2)=shrink;
        abc(2,2)=d;
        abc(3,2)=shrink;
        ab(1)='b';
        ab(2)='d';
        ab(3)='b';
    end
end
%%%Next, the value of d is determined that allows the area of the
%%%inclusion to be conserved/
for q=1:200
for p=1:N
    rtrans(p)=abc(1,2)*r(p);
end
for p=(N+1):M
    rtrans(p)=abc(2,2)*r(p);
end
for p=(M+1):i1
    rtrans(p)=abc(3,2)*r(p);
end
%%%Computes polar to cartesian and computes the area
[xincl1,yincl1]=pol2cart(alpha,rtrans);
areai=0.5*(trapz(xincl1,yincl1)-trapz(yincl1,xincl1));
deviation=100*(abs(areainclusion1)-abs(areai))/abs(areainclusion1);
if(abs(deviation)>1)
    d=d-0.005;

```

```

end
if (ab(1)=='d')
    abc(1,2)=d;
end
if (ab(2)=='d')
    abc(2,2)=d;
end
if (ab(3)=='d')
    abc(3,2)=d;
end
end
%%%Next, plots the original and the displaced inclusions on the same polar
%%%graph.
figure
polar(alpha,r)
hold on
polar(alpha,rtrans,'k')
figure
[xincllfinal,yincllfinal]=pol2cart(alpha,rtrans);
xincllfinalfinal=xincllfinal+centroidXl;
yincllfinalfinal=yincllfinal+centroidYl;
%%%Next, plot the shrunk [black] and original [blue] contours on the same
graph
plot(xwallfinal,ywallfinal,'k')
hold on
plot(xlumenfinal,ylumenfinal,'k')
hold on
plot(xincllfinalfinal,yincllfinalfinal,'r')
hold on
plot(xinclusion1,yinclusion1)
hold on
plot(xlumen,ylumen)
hold on
plot(xwall,ywall)
%%%Next, puts the points in a format that can be appended to the in file
xincllfinalt=xincllfinalfinal';
yincllfinalt=yincllfinalfinal';
zil=zeros(i1,1);
incllcoord=horzcat(zil,xincllfinalt,yincllfinalt);
coord=vertcat(coord,incllcoord);
% %%%%%%%%%%%%%%%%%%%%%%%%%%%%%%%%%%%%%%%%%%%%%%%%%%%%%%%%%%%%%%%
% %%%%%%%%%%%%%%%%%%%%%%%%%%%%%%%%%%%%%%%%%%%%%%%%%%%%%%%%%%%%%%%
%%%Next, preapres to generate the .in file
for m=1:(w+1+i1+i2+i3)
    F(m,1)=m;
    space(m,1)=' ';
end
Fstring=num2str(F);
coordstring=num2str(coord);
contour=horzcat(Fstring,space,coordstring);
contour

```

## B. Determining Area Using Green's Theorem

Let  $C$  be a simple, closed, piecewise smooth curve in the plane  $\mathbb{R}^2$ . Let  $D$  be the open two-dimensional region bounded by the curve  $C$ . Then, for any function  $\mathbf{F}=(f(x,y),g(x,y))$  defined on  $D$  and having continuous partial derivatives on  $D$ , Green's theorem states that

$$\int_C f dx + g dy = \iint_D \left( \frac{\partial g}{\partial x} - \frac{\partial f}{\partial y} \right) dA \quad (\text{B.1})$$

Now, for the double integral on the right hand side to represent the area of  $D$ , we need

$$\frac{\partial g}{\partial x} - \frac{\partial f}{\partial y} = 1 \quad (\text{B.2})$$

Choose  $\frac{\partial g}{\partial x} = 0.5$  and  $\frac{\partial f}{\partial y} = -0.5$ . Integrating with respect to  $x$  and  $y$  respectively, we get

$$g = 0.5x + C_1(y), \quad (\text{B.3})$$

$$f = -0.5y + C_2(x), \quad (\text{B.4})$$

where  $C_1(y)$  and  $C_2(x)$  are the two constants of integration.

Finally, choosing  $C_1(y) = 0$  and  $C_2(x) = 0$ , and substituting  $f$  and  $g$  in the left hand side of the eq.

B.1 gives an expression that can be used to compute the area of  $D$  using line integral:

$$\text{Area} = \frac{1}{2} \left( \int_C x dy - \int_C y dx \right) \quad (\text{B.5})$$

## C. Matlab Codes Used to Determine the Arterial Wall Thickness

```
%%%%%%%%%%%%%%%%%%%%%%%%%%%%%%%%%%%%%%%%%%%%%%%%%%%%%%%%%%%%%%%%%%%%%%%%Thickness Using Shortest Distance Method%%%%%%%%%%%%%%%%%%%%%%%%%%%%%%%%%%%%%%%%%%%%%%%%%%%%%%%%%%%%%%%%%%%%%%%%
%%%%%%%%%%%%%%%%%%%%%%%%%%%%%%%%%%%%%%%%%%%%%%%%%%%%%%%%%%%%%%%%%%%%%%%%Sayan Mondal%%%%%%%%%%%%%%%%%%%%%%%%%%%%%%%%%%%%%%%%%%%%%%%%%%%%%%%%%%%%%%%%%%%%%%%%
%%%%%%%%%%%%%%%%%%%%%%%%%%%%%%%%%%%%%%%%%%%%%%%%%%%%%%%%%%%%%%%%%%%%%%%%Matlab code, 2007 Edition%%%%%%%%%%%%%%%%%%%%%%%%%%%%%%%%%%%%%%%%%%%%%%%%%%%%%%%%%%%%%%%%%%%%%%%%
%%%%%%%%%%%%%%%%%%%%%%%%%%%%%%%%%%%%%%%%%%%%%%%%%%%%%%%%%%%%%%%%%%%%%%%%
figure
clear
f1=fopen('lumenCoord.txt','rt+') ; %lumen.txt contains the lumen coordinates
in pixels
lumen=fscanf(f1,'%e',[3,401]);
fclose(f1);
f2=fopen('wallCoord.txt','rt+') ;
wall=fscanf(f2,'%e',[3,401]);
fclose(f2);
%%%%%%%%%%%%%%%%%%%%%%%%%%%%%%%%%%%%%%%%%%%%%%%%%%%%%%%%%%%%%%%%%%%%%%%%
xlumen=lumen(2,:);
ylumen=lumen(3,:);
xwall=wall(2,:);
ywall=wall(3,:);
%%%%%%%%%%%%%%%%%%%%%%%%%%%%%%%%%%%%%%%%%%%%%%%%%%%%%%%%%%%%%%%%%%%%%%%%
arealumen=0.5*(trapz(xlumen,ylumen)-trapz(ylumen,xlumen)); %determines the
%area enclosed in the closed loop of the lumen using area formula derived
%from Green's theorem.
%%%%%%%%%%%%%%%%%%%%%%%%%%%%%%%%%%%%%%%%%%%%%%%%%%%%%%%%%%%%%%%%%%%%%%%%Determines the Centroid of the Original Lumen
g1=xlumen.*xlumen;
f1=ylumen.*ylumen;
centroidXl=0.5*trapz(g1,ylumen)/arealumen;
centroidYl=-0.5*trapz(f1,xlumen)/arealumen;
%%%%%%%%%%%%%%%%%%%%%%%%%%%%%%%%%%%%%%%%%%%%%%%%%%%%%%%%%%%%%%%%%%%%%%%%Converts wall and lumen coordinates to Polar, origin at the
%%%%%%%%%%%%%%%%%%%%%%%%%%%%%%%%%%%%%%%%%%%%%%%%%%%%%%%%%%%%%%%%%%%%%%%%centroid of the lumen%%%%%%%%%%%%%%%%%%%%%%%%%%%%%%%%%%%%%%%%%%%%%%%%%%%%%%%%%%%%%%%%%%%%%%%%
[alpha,rl]=cart2pol(xlumen-centroidXl,ylumen-centroidYl);
for p=1:401
alpha(2,p)=2*pi+alpha(1,p);
alpha(3,p)=4*pi+alpha(1,p);
end
[alphaw,rw]=cart2pol(xwall-centroidXl,ywall-centroidYl);
for p=1:401
alphaw(2,p)=2*pi+alphaw(1,p);
alphaw(3,p)=4*pi+alphaw(1,p);
end
dal=;%Input the valuse of dal to specify the angular region in which the code
will search for the shortest distance.
plot(xwall,ywall)
hold on
plot(xlumen,ylumen)
hold on
for q=1:4:401
k=0;
clear d dp
for p=1:401
```

```

    if(((alphaw(2,p)<(alpha(2,q)+dal))&&(alphaw(2,p)>(alpha(2,q)-
dal))))||((alphaw(2,p)<(alpha(3,q)+dal))&&(alphaw(2,p)>(alpha(3,q)-
dal))))||((alphaw(2,p)<(alpha(1,q)+dal))&&(alphaw(2,p)>(alpha(1,q)-dal))))
        k=k+1;
        d(k)=(((xwall(p)-xlumen(q))^2)+((ywall(p)-ylumen(q))^2))^0.5;
        dp(k)=p;
    end
end
[T(q),pp]=min(d);
pointw=dp(pp);
X(1)=xwall(pointw);
X(2)=xlumen(q);
Y(1)=ywall(pointw);
Y(2)=ylumen(q);
plot(X,Y,'k')
hold on
end
max(T)
k=0;
for l=1:4:401
    k=k+1;
    TH(k)=T(l);
end
THI=TH';
xlswrite('P323ICA_thickness_T1',THI,'A1:A101')%writes to the Excel file
%%%%%%%%%%%%%%%%%%%%%%%%%%%%%%%%%%%%%%%%%%%%%%%%%%%%%%%%%%%%%%%%%%%%%%%%

```

## D. Wall Thickness Increase vs. various components of the structural stress

This appendix presents the correlations between WTI and the yz component  $\sigma_{yz}$  of the stress tensor, the yz component  $L_{yz}$  of the left stretch tensor, and the yz component  $R_{yz}$  of the right stretch tensor at time 1 and time 2 respectively.

| Patient | Number of Points | $\sigma_{yz}$ | $L_{yz}$ | $R_{yz}$ |
|---------|------------------|---------------|----------|----------|
| 1       | 500              | 0.0960        | 0.101    | 0.0972   |
| 2       | 300              | -0.265        | -0.275   | -0.274   |
| 3       | 400              | -0.143        | -0.139   | -0.121   |
| 4       | 600              | 0.202         | 0.208    | 0.216    |
| 5       | 300              | 0.0838        | 0.0865   | 0.0805   |
| 6       | 500              | 0.211         | 0.227    | 0.219    |
| 7       | 400              | -0.260        | -0.251   | -0.210   |
| 8       | 500              | 0.214         | 0.147    | 0.128    |
| 9       | 300              | -0.0160       | -0.00857 | 0.00358  |
| 10      | 600              | -0.0860       | -0.0892  | -0.0947  |
| 11      | 600              | -0.0400       | -0.313   | -0.284   |

**Table D.1 Simple Pearson Correlation between Wall Thickness Increase and various Mechanical Variables (not including  $\sigma_{P1}$ ) at the Inner Wall at Time 1**

| Patient | Number of Points | $\sigma_{yz}$ | $L_{yz}$ | $R_{yz}$ |
|---------|------------------|---------------|----------|----------|
| 1       | 500              | 0.169         | 0.172    | 0.171    |
| 2       | 300              | -0.282        | -0.282   | -0.254   |
| 3       | 400              | -0.0848       | -0.0874  | -0.0706  |
| 4       | 600              | 0.159         | 0.156    | 0.135    |
| 5       | 300              | 0.321         | 0.201    | 0.194    |
| 6       | 500              | -0.0181       | 0.00221  | -0.0260  |
| 7       | 400              | 0.112         | -0.0270  | -0.0380  |
| 8       | 500              | 0.153         | 0.152    | 0.146    |
| 9       | 300              | 0.0332        | 0.0235   | 0.00735  |
| 10      | 600              | 0.0559        | 0.0616   | 0.0463   |
| 11      | 600              | -0.126        | -0.121   | -0.0618  |

**Table D.2 Simple Pearson Correlation between Wall Thickness Increase and various Mechanical Variables (not including  $\sigma_{P1}$ ) at the Inner Wall at Time 2**